

การเพิ่มสมบัติทางไฟฟ้าของพอลิเมทิลเมทาคริเลตสำหรับการประยุกต์เป็นเซลล์แสงอาทิตย์ชนิดสี
ย้อมไวแสง



บทคัดย่อและแฟ้มข้อมูลฉบับเต็มของวิทยานิพนธ์ตั้งแต่ปีการศึกษา 2554 ที่ให้บริการในคลังปัญญาจุฬาฯ (CUIR)
เป็นแฟ้มข้อมูลของนิสิตเจ้าของวิทยานิพนธ์ ที่ส่งผ่านทางบัณฑิตวิทยาลัย

The abstract and full text of theses from the academic year 2011 in Chulalongkorn University Intellectual Repository (CUIR)
are the thesis authors' files submitted through the University Graduate School.

วิทยานิพนธ์นี้เป็นส่วนหนึ่งของการศึกษาตามหลักสูตรปริญญาวิทยาศาสตรมหาบัณฑิต
สาขาวิชาปิโตรเคมีและวิทยาศาสตร์พอลิเมอร์
คณะวิทยาศาสตร์ จุฬาลงกรณ์มหาวิทยาลัย
ปีการศึกษา 2559
ลิขสิทธิ์ของจุฬาลงกรณ์มหาวิทยาลัย

ELECTRICAL PROPERTIES ENHANCEMENT OF POLY(METHYL METHACRYLATE) FOR DYE-
SENSITIZED SOLAR CELL APPLICATIONS

Miss Godchaporn Bunmee



A Thesis Submitted in Partial Fulfillment of the Requirements
for the Degree of Master of Science Program in Petrochemistry and Polymer Science

Faculty of Science

Chulalongkorn University

Academic Year 2016

Copyright of Chulalongkorn University

กชพร บุญมี : การเพิ่มสมบัติทางไฟฟ้าของพอลิเมทิลเมทาคริเลตสำหรับการประยุกต์เป็น เซลล์แสงอาทิตย์ชนิดสีย้อมไวแสง (ELECTRICAL PROPERTIES ENHANCEMENT OF POLY(METHYL METHACRYLATE) FOR DYE-SENSITIZED SOLAR CELL APPLICATIONS) อ.ที่ปรึกษาวิทยานิพนธ์หลัก: รศ. ดร.นพิตา วิทยุชिरะนันท์, อ.ที่ปรึกษา วิทยานิพนธ์ร่วม: ดร.ณัฐพล ภูตระกูลโชติ, 80 หน้า.

ปัจจุบันเซลล์แสงอาทิตย์ชนิดสีย้อมไวแสง (dye-sensitized solar cells, DSSC) ได้รับความสนใจเป็นอย่างมากในด้านของพลังงานทดแทนจากแสงอาทิตย์ เนื่องจากวิธีการประกอบที่ง่าย และให้ค่าประสิทธิภาพที่ดีพอควร เซลล์แสงอาทิตย์ชนิดสีย้อมไวแสงประกอบด้วยขั้วไฟฟ้าโปร่งแสง สารกึ่งตัวนำ สารละลายอิเล็กโทรไลต์ และสีย้อม โดยทั่วไปแล้วขั้วไฟฟ้าร่วมโปร่งแสงทำจากกระจก นำไฟฟ้าฟลูออรีนโดปทินออกไซด์ (fluorine-doped tin oxide, FTO) แต่กระจกชนิดนี้มีข้อเสียในด้าน มีความเปราะสูง น้ำหนักมาก และมีราคาแพง ดังนั้นในงานวิจัยนี้จึงเสนอที่จะใช้พอลิเมทิลเมทาคริเลต (poly(methyl methacrylate, PMMA) มาแทนที่กระจกนำไฟฟ้าฝั่งขั้วไฟฟ้าร่วม (counter electrode) เนื่องจากมีความโปร่งแสงสูง ราคาถูก และมีน้ำหนักเบา แต่แผ่นพลาสติกดังกล่าวไม่นำไฟฟ้า จึงต้องเพิ่มค่าการนำไฟฟ้าให้กับแผ่น PMMA ก่อนไปใช้ในเซลล์ DSSC โดยการเคลือบพอลิเอทิลีนไดออกซีไทโอฟีน (poly(3,4-ethylenedioxythiophene), PEDOT) ผ่านวิธีการปั่นเคลือบที่ความเร็วรอบ 300 รอบ/วินาที เป็นเวลา 30 วินาที พบว่าแผ่นพลาสติกมีความต้านทานลดลงจาก 10^{14} โอห์ม/ตร.ซม. เป็น 30.65 โอห์ม/ตร.ซม. และพบว่า PEDOT ยังมีศักยภาพในการเป็นตัวเร่งปฏิกิริยารีดอกซ์ (redox reaction) ของอิเล็กโทรไลต์ได้ดีอีกด้วย เมื่อทำการแทรกชั้นซิงก์ออกไซด์ (Zinc oxide, ZnO) ลงไประหว่างแผ่น PMMA และ PEDOT (PEDOT/ZnO/PMMA) แล้วนำไปประกอบเป็นขั้วไฟฟ้าร่วมในเซลล์ DSSC พบว่าเซลล์มีประสิทธิภาพสูงขึ้นถึงร้อยละ 150 เมื่อเทียบกับแผ่น PMMA ที่มีแต่ชั้น PEDOT เพียงอย่างเดียว (PEDOT/PMMA)

สาขาวิชา ปีโตรเคมีและวิทยาศาสตร์พอลิเมอร์ ลายมือชื่อนิสิต

ปีการศึกษา 2559

ลายมือชื่อ อ.ที่ปรึกษาหลัก

ลายมือชื่อ อ.ที่ปรึกษาร่วม

5671901023 : MAJOR PETROCHEMISTRY AND POLYMER SCIENCE

KEYWORDS: COUNTER ELECTRODE / POLY(METHYL METHACRYLATE) / POLY(3,4 - ETHYLENEDIOXYTHIOPHENE) / ZNIC OXIDE / DYE-SENSITIZED SOLAR CELL

GODCHAPORN BUNMEE: ELECTRICAL PROPERTIES ENHANCEMENT OF POLY(METHYL METHACRYLATE) FOR DYE-SENSITIZED SOLAR CELL APPLICATIONS. ADVISOR: ASSOC. PROF. NAPIDA HINCHIRANAN, Ph.D., CO-ADVISOR: NUTTAPOL POOTRAKULCHOTE, Ph.D., 80 pp.

Dye-sensitized solar cell (DSSC) have gained considerable attention in the field of solar energy due to their simplicity of fabrication and good efficiency. A DSSCs are consisted of transparent electrodes semiconductors, electrolyte solution and dye. Normally, the transparent electrodes are made from the fluorine-doped tin oxide glass (FTO-glass), but this glass type has drawback in terms of high brittleness, heavy weight and high cost. Thus, this research proposed the use of poly(methyl methacrylate) (PMMA) for replacing the FTO glass since it had excellent optical transparency, low cost and light weight. However, it is classified as non-conductive polymer. Therefore, the enhancement of electrical conductivity of PMMA sheet was required before applying in DSSC via spin coating of poly(3,4-ethylenedioxythiophene) (PEDOT) onto PMMA substrate at a spinning rate of 300 rpm for 30 s. It was found that the electrical resistance of PMMA sheet was reduced from $10^{14} \Omega/\text{cm}^2$ to $30.65 \Omega/\text{cm}^2$. In addition, PEDOT had potential to be the catalyst for redox reaction of electrolyte. When the zinc oxide (ZnO) layer was inserted between PMMA sheet and PEDOT (PEDOT/ZnO/PMMA sheet), it was observed that the DSSC consisting of PEDOT/ZnO/PMMA sheet provided the higher energy conversion efficiency as 150% than that of PEDOT/PMMA.

Field of Study: Petrochemistry and
Polymer Science

Academic Year: 2016

Student's Signature

Advisor's Signature

Co-Advisor's Signature

ACKNOWLEDGEMENTS

The author would like to express her greatest gratitude to her advisor, Associate Professor Dr. Napida Hinchiranan and co-advisor, Dr. Nuttapol Pootrakulchote, for their encouraging guidance, supervision and helpful suggestion during the course of this research. In addition, the author wishes to thank Assistant Professor Dr. Warinthorn Chavarisi, Assistant Professor Dr. Supaporn Noppakundilograt and Assistant Professor Dr. Warunee Ariyawiriyanan, for serving as the chairman and member of the thesis committee, respectively.

The author also thanks for the research financial supports from the Program in Petrochemistry and Polymer Science, Faculty of Science, Chulalongkorn University, Center of Excellence on Petrochemical and Materials Technology (PETROMAT) and Ratchadapisek Sompoch Endowment Fund (2013), Chulalongkorn University (Sci-Super 2014-028). The author wishes to express her thankfulness to Assistant Professor Dr. Sojiphong Chatraphorn, Department of Physics and technicians of the Department of Chemical Technology, Faculty of Science, Chulalongkorn University for providing their assistance throughout this research.

Thanks are going towards all of her friends in the laboratory for their friendships, assistance, suggestion, advice concerning the experimental techniques and the encouragement during the course of her graduate research.

Finally, and most of all, the author wishes to express her deepest gratitude to her family; especially, her parents for their love, support and encouragement throughout her entire study.

CONTENTS

	Page
THAI ABSTRACT	iv
ENGLISH ABSTRACT	v
ACKNOWLEDGEMENTS	vi
CONTENTS	vii
LIST OF TABLES	1
LIST OF FIGURES	2
CHAPTER I INTRODUCTION.....	1
1.1 The statement of problems	1
1.2 Objectives of the research.....	3
1.3 Research timeline	4
CHAPTER II THEORY AND LITERATURE REVIEW	6
2.1 Poly(methyl methacrylate) (PMMA)	6
2.2 Conductive polymers.....	7
2.3 Poly(3,4-ethylenedioxythiophene) (PEDOT)	9
2.3.1 Synthesis of in situ PEDOT.....	10
2.3.2 Physical properties	11
2.3.3 Chemical properties.....	11
2.3.4 Applications of PEDOT.....	13
2.3.5 Enhancement of PEDOT conductivity	14
2.4 Zinc oxide (ZnO)	14
2.5 Preparation of conductive polymer film.....	15
2.6 Solar cell.....	17

	Page
2.6.1 Silicon solar cell.....	17
2.6.2 Dye-sensitized solar cell (DSSC)	19
2.7 Operating principles and structure of DSSC	19
2.7.1 Cell structure.....	19
2.7.2 Dye sensitizer	20
2.7.3 Electrolyte solution.....	22
2.7.4 Titanium dioxide or titania (TiO ₂)	23
2.7.5 Counter electrode performance	24
2.8 Operating principles of DSSC.....	25
2.9 Literature reviews	27
CHAPTER III EXPERIMENTAL	31
3.1 Materials and chemicals.....	31
3.2 Preparation of PEDOT/PMMA sheets	32
3.3 Preparation of PEDOT/ZnO/PMMA sheets.....	33
3.4 Fabrication of DSSC	33
3.5 Characteristic and physical properties of the modified PMMA sheets	35
3.5.1 Structural characterization of PEDOT film on the modified PMMA sheets.....	35
3.5.2 Type and crystalline matter on PEDOT/ZnO/PMMA sheets.....	35
3.5.3 Morphology and topology of the modified PMMA sheets	35
3.5.4 Contact angle of surlyn and modified PMMA sheets	36
3.5.5 Electrical resistivity and conductivity of the modified PMMA sheets..	36
3.5.6 Catalytic activity of PEDOT for I ₃ ⁻ /I ⁻ redox	37

	Page
3.6 Electrochemical properties of DSSC	38
CHAPTER IV RESULTS AND DISCUSSIONS	40
4.1 Structural characterization of PEDOT deposited on the modified PMMA sheets	40
4.2 Initial study of suitable EDOT monomer concentration and spinning time for preparation of modified PMMA sheets	41
4.3 Effect of spinning rate, number of EDOT layers and 2-methylimidazole content on electrical resistance and appearance of modified PMMA sheets	43
4.4 Effect of zinc oxide layer on the properties of modified PMMA sheets	45
4.4.1 Crystalline structure of ZnO colloidal.....	46
4.4.2 Energy dispersive X-ray spectroscopy (EDS) of ZnO/PMMA sheets	47
4.4.3 Morphology, topology and electrical resistance of PMMA/ZnO/PMMA sheets (modified PMMA sheets)	48
4.5 Electrochemical properties of modified PMMA counter electrode measured by cyclic voltammetry (CV).....	51
4.6 Performance of DSSC based on FTO and different counter electrodes	54
4.7 Incident photo-to-current efficiency (IPCE)	58
CHAPTER V CONCLUSION	60
5.1 Conclusion.....	60
5.1.1 Enhancement of electrical conductivity of poly(methyl methacrylate) (PMMA) sheet via spin coating of 3,4-ethylnedioxythiophene (EDOT) monomer	60
5.1.2 Effect of zinc oxide layer on the properties of modified PMMA sheets (PEDOT/ZnO/PMMA sheets)	60

	Page
5.1.3 Performance of DSSC.....	61
5.2 Recommendations.....	61
REFERENCES	63
APPENDIX.....	70
APPENDIX A	71
APPENDIX B	72
APPENDIX C	73
APPENDIX D.....	74
APPENDIX E.....	78
VITA.....	80



LIST OF TABLES

Table 2.1	Selected physical properties of EDOT.....	12
Table 2.2	Physicochemical properties of Z-907	21
Table 3.1	Recipe for preparation of PEDOT/PMMA sheets.	32
Table 4.1	Effect of EDOT monomer content and spinning time on electrical resistance and appearance of the modified PMMA sheets	42
Table 4.2	Effect of spinning rate on PEDOT film thickness and electrical resistance and appearance of PEDOT/PMMA sheets	44
Table 4.3	Effect of number of PEDOT layers and 2-methylimidazole content on electrical conductivity of modified PMMA sheets	45
Table 4.4	The effect of ZnO concentration in the PMMA syrup on the roughness and electrical resistance of the modified PMMA sheets.....	51
Table 4.5	Electrochemical characteristics of Pt, bare FTO, PEDOT and PEDOT/ZnO electrodes	54
Table 4.6	Photovoltaic performance of DSSC using various kinds of counter electrode	56
Table 4.7	The contact angle of water on the surface of surlyn, PEDOT/ZnO/PMMA sheet, 2-methylimidazole/PEDOT/ZnO/PMMA sheet.....	57

LIST OF FIGURES

Figure 2.1	Chemical structure of PMMA.....	6
Figure 2.2	The band gap diagram of insulators, semiconductors and conductors	8
Figure 2.3	Chemical structures of (a) 3,4-Ethylenedioxythiophene (EDOT) and (b) poly(3,4-ethylenedioxythiophene) (PEDOT).	9
Figure 2.4	Schematic of <i>in situ</i> PEDOT synthesis.	11
Figure 2.5	Acid catalyzed dimerization and trimerization EDOTn.	13
Figure 2.6	The structure of crystalline silicon solar cell.....	18
Figure 2.7	Schematic representation of DSSC.	20
Figure 2.8	Dye sensitizers derived from ruthenium polypyridyl complexes.	21
Figure 2.9	Band positions of several semiconductors in contact with aqueous electrolyte (red color = lower edge of the conduction band and green color = upper edge of the valence band).	23
Figure 2.10	Titania phases (a) rutile, (b) anatase and (c) brookite.....	24
Figure 3.1	Schematic diagram of DSSC preparation using the modified PMMA sheet acting as the counter electrode.....	34
Figure 3.2	Cross-section of assembled DSSC module.	35
Figure 3.3	Four-point probe conductivity cell.....	37
Figure 3.4	I-V characteristic of an illuminated solarcell.....	39
Figure 4.1	ATR-FTIR spectrum of the PEDOT deposited on the PMMA sheet compared to that of PEDOT powder.....	41

Figure 4.2	SEM images of the cross-section of PEDOT film on PMMA sheet obtained from various spinning rates: (a) 300 rpm, (b) 500 rpm and (c) 1,000 rpm.....	43
Figure 4.3	XRD pattern image of ZnO.	47
Figure 4.4	EDS spectrum of ZnO coated on the PMMA sheets: (a) 0.41, (b) 0.76 and (c) 3.03 wt% ZnO on PMMA sheets.	48
Figure 4.5	SEM images of the cross-section of the PEDOT/ZnO/PMMA sheets prepared by using various ZnO concentrations in the PMMA syrup: (a) 0 wt%, (b) 10 wt%, (c) 34 wt% and (d) 58 wt%.	49
Figure 4.6	AFM and SEM images of (a) PEDOT/PMMA sheets and PEDOT/ZnO/PMMA sheets obtained from (b) 10 wt% (c) 34 wt% and (d) 58 wt% ZnO concentration in the PMMA syrup.	50
Figure 4.7	Cyclic voltammograms of (a) Pt counter electrode and (b) PEDOT/ZnO/FTO (prepared from 10 wt% ZnO in PMMA syrup) compared to FTO with and without Pt at a scan rate of 20 mV/s in 0.01M LiI and 0.001M I ₂ in acetonitrile solution containing 0.1M LiClO ₄ used as the supporting electrolyte.	52
Figure 4.8	Comparative I-V curves of DSSC with different counter electrodes made from FTO glass, PEDOT/glass, PEDOT/PMMA, and PEDOT/ZnO/PMMA (10 wt% ZnO in the PMMA syrup).....	55
Figure 4.9	IPCE of DSSC with modified PMMA sheet and Pt counter electrode.	59

CHAPTER I

INTRODUCTION

1.1 The statement of problems

The energy crisis and global warming problem caused by the use of conventional fossil fuels have been motivating all countries to develop the technology for renewable energy. Dye-sensitized solar cell (DSSC) has been intensively investigated over the past few decades as an alternative solar energy converter due to its easier fabrication, lower operation cost with equivalent conversion efficiency compared to conventional silicon solar cells (Kim et al. 2006; Chen, Wei, and Ho 2007). A typical DSSC device consists of two electrodes made from transparent conductive glasses. One is a dye-sensitized titanium dioxide (TiO₂) photoanode used for absorbing visible light (Wu et al. 2008); whilst, the platinum (Pt)-coated conductive glass is used as counter electrode for catalyzing the reaction of tri-iodide to iodide ($I_3^- + 2e^- \leftrightarrow 3I^-$) redox electrolyte (Sakurai et al. 2009).

Considering the cost of DSSC production, the fluorine-doped tin oxide layer glass (FTO-glass), a general conductive substrate applied in DSSC, accounts for approximately 20 – 60% of the total cost of DSSC modules (Kavan et al. 2016). Moreover, poor flexibility and limitation of availability of FTO-glass are the great barriers to commercialization (Sahito et al. 2016). Other materials have been searched to replace the FTO-conductive glass in DSSC. For example, Yun et al. (2012) reported that a Pt-coated titanium (Ti) foil and a perforation-patterned stainless steel (StSt) could be applied as the counter electrode and photoanode, respectively. The overall conversion efficiency of this system was in the range of 1.02 – 2.25% depended on the perforation pitches. Sahito et al. (2016) prepared the flexible and conductive cotton

fabric electrode coated with graphene nanosheets (HC-GCF) as the counter electrode for DSSC. It was found that the DSSC made from HC-GCF provided 6.93% overall conversion efficiency, which is slightly lower than that of the conventional Pt-based DSSC on FTO-glass (8.44%). Furthermore, the conductive polymers such as polyimide containing conductive carbon (CC/PI) (Zhou et al. 2013) and polyethylene naphthalate coated with tin oxide (ITO-PEN) (Wu et al. 2016) were used as the counter electrode for the flexible DSSC, showing the overall conversion efficiencies of DSSC of 2.02% and 1.55%, respectively.

Among available transparent commodity engineering plastics, poly(methyl methacrylate) (PMMA) has potential to replace FTO-glass for its light weight, high optical transparency, environmental durability, good impact resistance and low price (Zhang et al. 2011). However, PMMA is classified as a non-conductive polymer. Thus, it cannot be directly applied as electrode for DSSC. To enhance the conductivity of PMMA, poly(3,4-ethylenedioxythiophene) (PEDOT), one of conducting polymers with high conductivity, electrochemical stability and ability to produce as film on large areas (Hansen et al. 2006; Xiao et al. 2012), was selected to modify the surface of PMMA via *in situ* polymerization of 3,4-ethylenedioxythiophene (EDOT) using iron (Fe) (III) tosylate as an oxidant (Hansen et al. 2006). 2-Methylimidazole in ethanol was also introduced during the surface modification of PEDOT-coated PMMA (PEDOT/PMMA) in order to rearrange the PEDOT segments expected to achieve the better connection between the PEDOT chains (Saghaei, Fallahzadeh, and Yousefi 2015).

PEDOT is not only used as a conductive polymer, but it also acts as catalyst for I_3^-/I^- redox reaction in DSSC. It has been reported that the combination of zinc oxide (ZnO) and PEDOT used as the DSSC counter electrode exhibits the maximum power conversion efficiency as 8.17% since the interaction energy of I_3^- and ZnO (30 kcal/mol) is higher than that of I_3^- and PEDOT alone (8.4 kcal/mol) (Xia et al. 2007). Thus, the integration of ZnO and PEDOT has great potential to replace the expensive

Pt catalyst generally used as catalyst for I_3^- reduction. In addition, ZnO is an attractive semiconductor due to its wide band gap (3.2 eV), easy synthesis, low cost and non-toxicity. It also shows the ultraviolet absorption behavior, which can be applied as ultraviolet (UV)-shielding material. From these advantage properties, ZnO is suitable for large scale applications (Wang, Wei, and Hu 2013).

Thus, the objective of this work is to prepare the conductive PMMA via *in situ* polymerization of PEDOT using spin coating technique. The obtained PEDOT/PMMA sheet was applied as the counter electrode in DSSC without the use of Pt catalyst. The effect of spinning rate and spinning time of EDOT solution, EDOT concentration and 2-methylimidazole content on PEDOT film thickness and electrical resistivity of PEDOT/PMMA sheets was observed. Moreover, the topology and the overall energy conversion efficiency of DSSC made from PEDOT/PMMA sheets as counter electrode with and without the assistance of ZnO layer were also compared and reported.

1.2 Objectives of the research

The objectives of this research are stated as follows:

- 1.2.1 To prepare the conductive PMMA sheets via *in situ* polymerization of EDOT using spin coating technique.
- 1.2.2 To study the effect of spinning rate and spinning time of EDOT solution, EDOT concentration and 2-methylimidazole content on PEDOT film thickness and electrical resistivity including the topology of PEDOT/PMMA sheets with and without the assistance of ZnO layer.
- 1.2.3 To investigate the overall energy conversion efficiency of PEDOT/PMMA- or PEDOT/ZnO/PMMA-based DSSC.

1.3 Research timeline

The stepwise investigation is carried out as follows:

- 1.3.1 Review related research works
- 1.3.2 Synthesize PEDOT/PMMA sheets via *in situ* polymerization of EDOT using spin coating technique. Variable parameters were listed as shown below:
 - Spinning time (s): 15, 30, 45 and 60
 - Spinning rate (rpm): 300, 500 and 1,000
 - Concentration of EDOT monomer (M): 0.12, 0.24 and 0.72
 - Concentration of 2-Methylimidazole in ethanol (M): 1-6
- 1.3.3 Prepare ZnO solution was prepared via sol-gel technique.
- 1.3.4 Prepare the PEDOT/ZnO/PMMA sheets by spin coating technique and varying the volume of ZnO colloids (1-5 mL) and numbers of PEDOT layer coated on ZnO/PMMA sheets (1-3 layers).
- 1.3.5 Measure the properties of the obtained PEDOT/PMMA sheet and PEDOT/ZnO/PMMA sheet as followed:
 - Electrical resistivity: Standard four-point probe
 - Functional groups on the surface of the modified PMMA sheets: Attenuated total reflectance Fourier transform infrared (ATR-FTIR)
 - Morphology and thickness of the PEDOT or ZnO layers: Scanning electron microscope (SEM)
 - Topology of the surface of the modified PMMA sheets: Atomic force microscopy (AFM)

- Type and crystalline matter of ZnO on PEDOT/PMMA sheets: X-ray diffraction (XRD) and energy dispersive x-ray spectroscopy (EDS)
 - Catalytic activity of PEDOT for I^-/I_3^- redox: Cyclic voltammetry (CV)
- 1.3.6 Fabricate DSSC test devices based on novel materials and measure their photovoltaic characteristics by IV-tester.
- 1.3.7 Discuss results and prepare the thesis book and manuscript.



CHAPTER II

THEORY AND LITERATURE REVIEW

2.1 Poly(methyl methacrylate) (PMMA)

PMMA is one of the methacrylic resins, named acrylic resin. PMMA is a transparent thermoplastic showing the resistance properties to impact energy, weather and chemical. Moreover, it is known as a substitute for inorganic glass. PMMA stands out from other plastics since it has light weight (density = 1.17-1.20 g/cm³) with high light transmission (92%) and unlimited coloring options. (Goseki and Ishizone 2015). In addition, it shows the greatest surface hardness among all thermoplastics. It can be fabricated by all thermoforming methods, and therefore offers huge creative scope. Another major benefit is that PMMA is 100% recyclable, which makes an essential contribution to save natural resources (Subramanian 2014).

The most famous application of PMMA is the production of patio roofs and conservatories requiring high resistance to sun, rain and snow. It is also widely used in the automotive parts such as exterior and interior lighting, instrument covers, spoilers and mirror housings. PMMA is also used for lighting system such as light guide panels in backlight units for LCD display screens, lenses for mobile phones, rear projection and touch screens, illuminated signs, street lighting and industrial lamps. The chemical structure of PMMA is shown in Figure 2.1.

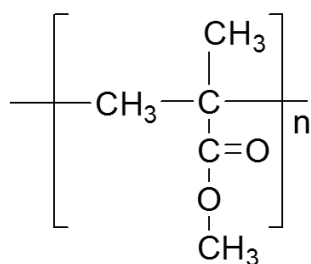


Figure 2.1 Chemical structure of PMMA.

2.2 Conductive polymers

Conductive polymers (CPs) are polymers that conduct electricity as electrical semiconductors due to the alternating single and double carbon-carbon bonds along the polymer backbone. CPs have been widely investigated and applied in various applications such as sensor, supercapacitors, energy storage devices, dye-sensitized solar cell (DSSC) and others. Moreover, CPs are easily synthesized and they have high conductivity, environmental stability, cost effectiveness and unique electrochemical redox properties (Saranya, Rameez, and Subramania 2015). Polythiazyl $(SN)_x$ is the first conjugated polymer, which was discovered in 1975. It exhibited metallic conductivity as well as superconductivity. Normally, CPs are mainly synthesized using either chemical oxidative polymerization or electrochemical polymerization. They have good conductivity in the range from a few S/cm to 500 S/cm in doped state with specific electronic, magnetic and mechanical properties (Mastragostino, Arbizzani, and Soavi 2002).

The examples of CPs are polyacetylene (PA), polyaniline (PANI), polypyrrole (PPy), poly(p-phenylenevinylene) (PPV), poly(3,4-ethylenedioxythiophene) (PEDOT), polyfuran (PF) and other polythiophene (PTh) derivatives. They can be used as thin film transistors (Kraft, Grimsdale, and Holmes 1998), polymer light emitting diodes (LEDs), corrosion resistance materials and electrochromic devices.

Figure 2.2 illustrates the energy diagram according to the band gap model. In the case of insulators, the valence band is fully occupied with electrons due to the covalent bonds. Electrons cannot move because they are "locked up" between atoms. To increase the conductivity of insulators, electrons from the valence band have to move across a large band gap into the conduction band. Only with considerable energy expenditure (if at all possible), the band gap can be overcome and lead a negligible conductivity. Semiconductors have much narrower band gap compared to insulators.

Thus, even at room temperature electrons from the valence band can be excited into the conduction band, where electrons can freely move and act as charge carriers. In addition, each electron also leaves behind a hole in the valence band, which can be filled by other electrons in the valence band. Thus, the holes are able to transport in the valence band and can be viewed as positive charge carriers. For the conductors, the filled valence band overlaps with the empty conduction band. In general, both states occur at the same time. Electrons can move inside the partially filled valence band or inside two overlapping bands. Thus, the band gap between the valence band and conduction band are not observed in the conductors.

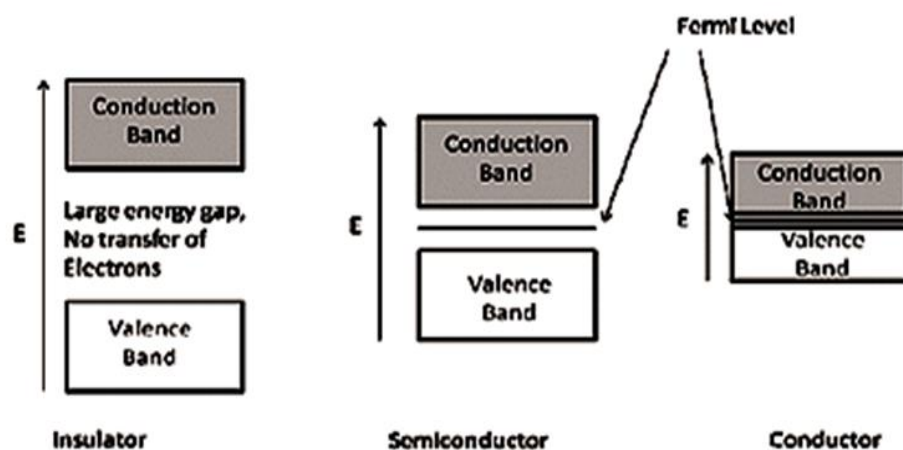


Figure 2.2 The band gap diagram of insulators, semiconductors and conductors

(Fine et al. 2010).

2.3 Poly(3,4-ethylenedioxythiophene) (PEDOT)

PEDOT is counted as the conductive polymer family. It is well-known for using as electrochemical p-dopant (or n-dopant) to oxidize (or reduce) the backbone polymer resulting in an increased electronic conductivity and structural transitions to give rise to spectral changes (Groenrndaal et al. 2003). The structure of 3,4-ethylenedioxythiophene (EDOT) and PEDOT are shown in Figure 2.3.

PEDOT has been extensively investigated for its high conductivity property to use as hole injecting layers in light emitting diodes (LEDs), solar cells and other semiconductor devices. PEDOT has been developed into one of the most successful materials from both fundamental and practical perspectives. It possesses several advantageous properties as compared with other polythiophene derivatives. It combines a low oxidation potential and moderate band gap with good stability in the oxidized state. In addition to a high conductivity, PEDOT is found to be highly transparent in thin oxidized films. As a result, PEDOT derivatives are now utilized in several industrial applications including antistatic coatings for photographic films, electrode material in solid-state capacitor and hole conducting material in organic/polymer-based light-emitting diodes (OLEDs/PLEDs) (Groenrndaal et al. 2000).

PEDOT has been commercialized. The PEDOT films were almost transparent which makes them suitable in applications as electrochromic display and antistatic transparent films.

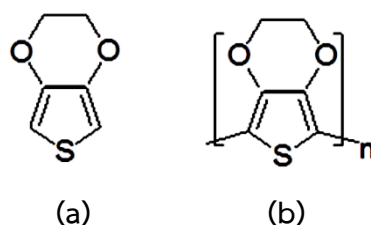


Figure 2.3 Chemical structures of (a) 3,4-Ethylenedioxythiophene (EDOT) and (b) poly(3,4-ethylenedioxythiophene) (PEDOT).

2.3.1 Synthesis of *in situ* PEDOT

In situ PEDOT can be synthesized under film-forming conditions. The oxidative *in situ* polymerization is carried out in the presence of ionic oxidants or similar metal ions in a suitable higher oxidation state. There are various metal salt oxidants and also completely distinct compounds. For example, peroxides. Fe-(III) is the oxidant preferred in most experiments in previous literatures and it is also predominant in the industrial use. The solubility of Fe-(III) oxidants is determined by the limited solubility of EDOT in water, which is contrast to its miscibility in alcohols such as ethanol or n-butanol in any ratios. Therefore, the alcohol soluble Fe salts of sulfonic acids are preferred to be used as oxidants. Especially, p-toluenesulfonate (Tos^-) has been established as a very suitable anion with respect to solubility and reactivity of the corresponding Fe-(III) salt. Thus, Fe-(III) toluenesulfonate (FeTos_3) has become the most widely used oxidant for EDOT in the preparation of *in situ* PEDOT layers for both laboratory and commercial scales (Elschner et al. 2011).

The overall reaction is described as shown in Figure 2.4. To illustrate a clearer picture, the equation is drawn for the EDOT, typically representing every third thiophene ring as a cationic moiety. The overall polymerization reaction is consisted of two steps. The first step is the oxidative polymerization of EDOT to produce the neutral PEDOT. p-Toluenesulfonic acid (TosH) and Fe-(II) p-toluenesulfonate (FeTos_2) are also stoichiometrically formed as by-products. Thus, two equivalents of Fe-(III) tosylate are necessary for this reaction. In the second step, the neutral PEDOT is doped by the action of “excess” Fe-(III) tosylate. As every third or fourth thiophene moiety loses one electron to form the cationic structure, FeTos_3 are needed for efficient doping. Here also the corresponding stoichiometric amount of Fe-(III) tosylate is formed. The third tosylate anion is incorporated into the polymer structure as the counterion. As the result, the *in situ* PEDOT layers formed by this two-step reaction

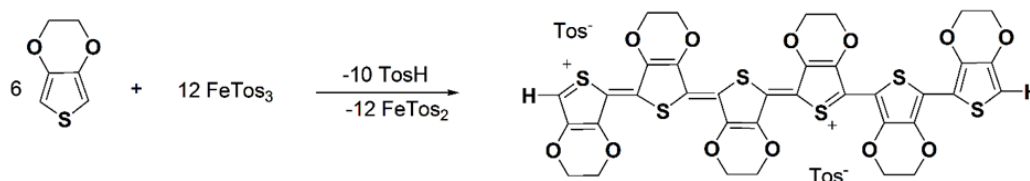


Figure 2.4 Schematic of *in situ* PEDOT synthesis (Elschner et al. 2011).

are initially containing Fe-(III) tosylate and toluenesulfonic acid. Both species can be removed by rinsing with water.

The neutral PEDOT can be isolated in traces to moderate amounts. For example, the use of Fe-(III) chloride instead of the Fe-(III) tosylate is not suitable for technical applications due to the formation of corrosive HCl and deeply colored tetrachloroferrate counterions resulting in the moderate yield of the neutral PEDOT (Kirchmeyer and Reuter 2005).

2.3.2 Physical properties

EDOT is a nearly colorless liquid with an unpleasant odor. A small change in color to pale yellow is possible after extended storage, especially in the daylight, without significantly affecting the analytical purity. The inhibition or decrease in these effects by base treatment has been described in a patent application. Some physical data including flash point and ignition temperature are given in Table 2.1 (Elschner et al. 2011).

2.3.3 Chemical properties

The most remarkable EDOT reaction is its oxidation reaction, typically resulting in conductive oligomer to polymer materials in the presence of charge balancing, so-called doping counterions (anions). There are several reaction pathways, but some reactions do not produce the conductive polythiophenes. Nevertheless, a lot of them

Table 2.1 Selected physical properties of EDOT (Elschner et al. 2011)

Viscosity (20 °C)	11 mPa.s
Density (20 °C)	1.34 g/cm ³
Melting point	10.5 °C
Boiling point (1013 mbar)	225 °C
Vapor pressure (20 °C)	0.05 mbar
Vapor pressure (90 °C)	10 mbar
Solubility in water (20 °C)	2.1 g/l
Flash point	104 °C
Ignition temperature	360 °C

is closely related to the essential EDOT chemistry that can form oligomers or polymers with electrical activity.

From the reaction mechanism as shown in Figure 2.5, the important feature is the ability of EDOT and a limited number of derivatives for protonation at α -position of the thiophene ring (species 1) by strong acids (H^+). For example, the protonation performed in the presence of sulfuric acid, organic sulfonic acids, or trifluoroacetic acid yields the formation of an active electrophilic $[EDOT-H]^+$ intermediate (species 2). Hydrochloric acid leads additional side reactions, while trichloroacetic acid is less active than the fluoro acid analogy. The $[EDOT-H]^+$ (species 2 or 3) is able to reversibly add to the basic C-2 of another EDOT molecule (species 4). The new formed intermediate may be deprotonated and produces dimeric structure such as 1,4-dihydrothiophene derivative (species 5) (Reuter et al., 2002). Because the C-5 in the dimeric product is also easily protonated, the reaction does not stop at the stage of this dimer, but another EDOT molecule is then added and produces the trimeric structure (species 6). Due to the reversibility of all steps, a quantitative yield of EDOT dimer or trimer is not

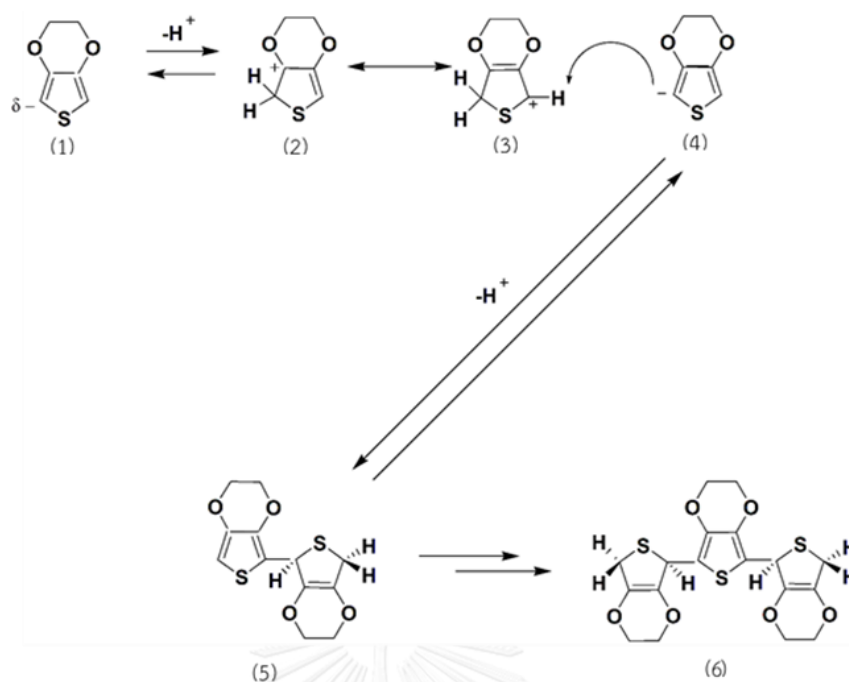


Figure 2.5 Acid catalyzed dimerization and trimerization EDOTn (Elschner et al. 2011).

achievable and an equilibrium state with the trimer as the minor component is established.

2.3.4 Applications of PEDOT

PEDOT has many excellent properties for using in a wide range of applications due to its low oxidation potential, moderate band gap, high conductivity and stability in the doped state. Thus, PEDOT can be applied as solar cells, antistatic and electrostatic coatings for metallization of insulators, and electrodes for capacitors or photodiodes. If the durability of the capacitors using PEDOT is enhanced, it will have a wider range of applications in electronic circuits for cars and man-made satellites. Since PEDOT is able to be doped and undoped, it is very attractive for electrochromic applications. With proper choice of counter-ions, PEDOT is also interest for applying as an electrochemical actuator (Elschner et al. 2011).

2.3.5 Enhancement of PEDOT conductivity

Conductive polymeric materials have gained considerable attention over the past several years because of their applications in novel optoelectronic devices such as photovoltaic devices and thin-film transistors. Among these materials, PEDOT is the most successful conductive polymer in commercial applications. Recently, several approaches have been reported to significantly improve the conductivity of PEDOT. To enhance the conductivity of PEDOT, the addition of different organic compounds or called as secondary dopands or additives such as several alcohols (diethylene glycol, glycerol, or sorbital) and high-boiling-point solvents (dimethyl sulfoxide, tetrahydrofurane, and dimethylformamide) was studied (Groenrndaal et al. 2000). The post-treatment to increase the conductivity of the PEDOT films by using 2-methylimidazol can rearrange the PEDOT segments leading the better connections between the conducting PEDOT chains.

Saghaei et al. (2015) reported that the electrical conductivity of PEDOT:poly(styrene sulfonate) (PSS) films was significantly improved without losing the optical transparency by treating the films with the solution of 2-methylimidazole in ethanol. The maximum electrical conductivity of a such thin film reached to 930 S/cm, which was higher than that of the pure PEDOT:PSS film (electrical conductivity = 0.8 S/cm).

2.4 Zinc oxide (ZnO)

ZnO is a semiconductor with wide direct band-gap. The crystalline structure of ZnO is in the form of hexagonal of wurtzite. ZnO is a very promising material for flexible electronic devices (FEDs), which is attractive for large commercial and scientific interest. It combines a wide range of benefits such as high electrical conductivity, piezoelectricity, easy fabrication, low cost, non-toxicity, ultraviolet absorption behavior

and it is also compatible with large scale applications (Fortunato et al. 2005; Pimentel et al. 2005). In addition, ZnO can be functionalized and combined in the organic–inorganic materials. Furthermore, the nanostructured ZnO is a promising candidate as an electron acceptor and a transport material for dye-sensitized solar cell (DSSC). The chemical stability of ZnO is less than that of TiO₂, which was found to be problematic in the dye adsorption procedure. Thus, DSSC containing overdose of dye loading having high acidity derived from carboxylic acid causes the dissolution of ZnO leading the poor overall electron injection efficiency (Quintana et al. 2007).

From the previous literature (Wang, Wei, and Hu 2013), ZnO is expected to have a strong interaction with the ions of iodine-based electrolytes resulting in the excellent catalytic activity. However, ZnO possesses poor electrical conductivity. Thus, it is necessary to combine ZnO with a conductive component such as a PEDOT:PSS.

2.5 Preparation of conductive polymer film

Various techniques have been developed to prepare conductive polymer films. These techniques include:

Electrochemical deposition: Electrochemical deposition is the most convenient method to deposit conductive polymer films onto the substrates. The thickness of the film can be controlled via the total charge passed through the electrochemical cell during film growing process. Moreover, the film can be deposited on patterned microelectrodes (Lu, Qu, and Shi 2005). The deposition must be carried out on a conducting substrate.

Spincoating: Nowadays, the film-forming technique employed for producing the polymer solar cells is spincoating. The technique is subjected to numerous fundamental studies and its use and scope has been reviewed recently. In spite of the complexity of film formation, this technique shows the high reproducibility to form

films and it also provides the homogeneous films over a large area when it is compared to other coating techniques. The spincoating technique is applied in the microelectronics industry such as the deposition of photoresistant polymer onto and the silicon wafers and crucial steps during the production of digital versatile discs (DVDs) and compact discs (CDs). The typical spincoating operation involves application of a liquid to a substrate followed by acceleration of the substrate to a chosen rotational speed. Alternatively, the liquid solution may be applied while the substrate is spinning. The angular velocity of the substrate with the overlying solution results the ejection of the most of the applied liquid to provide only thin film onto the substrate. The thickness, morphology and surface topography of the final film obtained from a particular material in a given solvent at a given concentration is highly reproducible. These three properties are also depended on rotational speed, viscosity of solution, volatility, diffusivity, molecular weight and concentration of the solutes (Krebs 2009).

Doctor blading: A little explored technique in the context of polymer solar cells is doctor blading to form films with a well-defined thickness (Schilinsky, Waldauf, and Brabec 2006; Mens et al. 2008). In contrast to the spincoating, this technique is quite parsimonious to minimize the loss of coating solution (loss less than 5%). The technique uses a sharp blade, which is placed on the desired position to deposit the thin film with 10-500 μm thickness. The coating solution is then put on the top of front blade and then linearly moved across the substrate. A thin wet film is left after casting. The final thickness of the wet film is ideally half of the gap width, but it may vary due to the surface energy of the substrate, the surface tension and viscosity of the coating solution. The final thickness of the wet film is also depended on the meniscus formed between the blade and the wet film on the trailing edge of the blade. This is related to the shear field which is proportional to the speed of the blade or knife. Although this technique ideally shows no loss of coating solution, the loss of coating solution is still found for the practical process. The loss of coating solution is large and thus gives

no advantage over spincoating. Furthermore, the film formation by doctor blading technique is slower than that by the spincoating technique. The aggregation of the dissolved material in the coating solution at high concentration is often happened during doctor blading (Krebs 2009).

Screen printing: The screen printing technique was developed at the beginning of the 20th century. This technique provides full 2-dimensional pattern of the printed layer with no loss of coating solution during printing. Its main distinction from all other printing and coating techniques is a large wet film thickness and a requirement for a relatively high viscosity and a low volatility of the coating solution. The process can be applied for screening the woven materials (i.e. synthetic fibre or steel mesh) glued on a frame under tension. The pattern of screen printing is obtained by filling the screen with an emulsion that is impervious to the coating solution in the areas where no print should appear. The screen is then filled with coating solution and then the coating solution is casted onto the surface of substrate by using a squeegee.

2.6 Solar cell

2.6.1 Silicon solar cell

In 1954, photovoltaic technology was invented in the United States when Daryl Chapin, Calvin Fuller, and Gerald Pearson developed the first silicon photovoltaic (PV) cell. The first solar cell was capable to convert enough sun energy into power to run electrical equipment everyday. The first silicon solar cell had only 4% efficiency and it has been improved to achieve 11% efficiency. Photovoltaic energy conversion in solar cells consists of two essential steps. First, absorption of light generates an electron and hole pairs. The electron and hole are then separated by built-in electric field across p-n junction thus generating electrical power. This process is illustrated as

show in Figure 2.6, which is the principal features of the typical solar cells used nowadays.

The produced in Figure 2.6, the structure has to be satisfied by adding suitable dopants like Boron or Phosphorous. If phosphorous is added, the doping (mixing impurities in order to make the material conductive) process is called n-doping. On the other hand, if Boron is added, the process is called p-doping. The n-doping is more effective than the p-doping. In n-doping, the electron will be allowed to move freely thus creating the ability to transfer charges. But in the p-doping, the vacancy filled will be regenerated in a new place causing further intrinsic conduction. If both the p area and the n area are brought together, the structure will be known as the p-n junction, this junction facilitates the movement of n-ions to the positive and p-ions to the negative region forming an electric field in the process. This electric field can be withdrawn and it can be used to power any electrical applications. So, technically this p-n junction is called the Solar Cell in this case (Markvart and Castañer 2013).

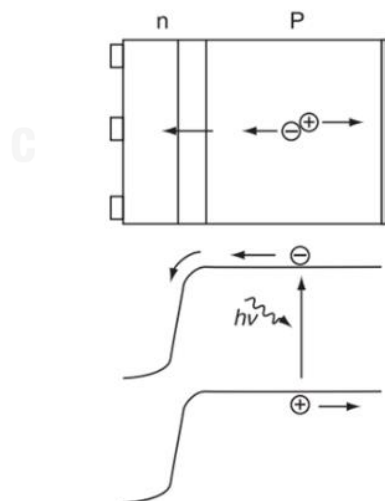


Figure 2.6 The structure of crystalline silicon solar cell (Markvart and Gastañer, 2013).

2.6.2 Dye-sensitized solar cell (DSSC)

The history of DSSC has been started since 1992. It is attractive because of its low cost, easy preparation and environmental friendliness. The DSSC offers a promising mean of harvesting the sun's energy and the improvement of its efficiency has drawn the interest of theoretical chemists and physicists.

DSSC differs from conventional semiconductor devices in that it separates the function of light absorption from the transportation of charge carrier. Dye sensitizer absorbs the incident sunlight and exploits the light energy to induce vector electron transfer reaction. Therefore, this system has been described in terms of artificial photosynthesis (O'Regan and Grätzel 1991). Like the chlorophyll in plants, a monolayer of dye molecules (sensitizer) absorbs the incident light. DSSC has the following advantages comparing with the silicon (Si) based photovoltaic (Wei 2010) as seen below:

- (1) It is not sensitive to the defects in semiconductors such as defect in Si.
- (2) The semiconductor electrolyte interface (SEI) is easy to form and it is cost effective for production.
- (3) It is possible to realize the direct energy transfer from photons to chemical energy.

2.7 Operating principles and structure of DSSC

2.7.1 Cell structure

Majority of high-efficient DSSC is consisted of the thin film derived from titanium dioxide (TiO_2) used as a photoanode and Pt electrode acting as a counter electrode. They are separated by liquid electrolyte (iodide/triiodide (I^-/I_3^-) redox couple). Both electrodes are made of fluorine -dope SnO_2 layer glass (FTO-glass). The components in the DSSC module is presented in Figure 2.7.

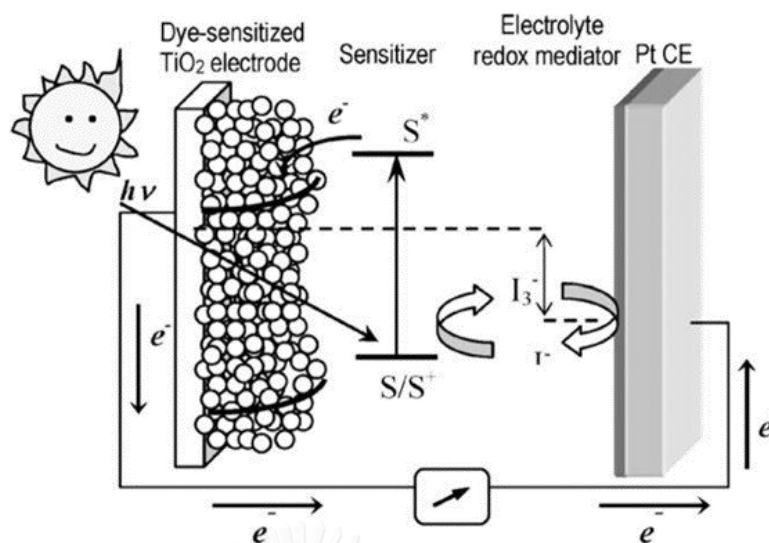


Figure 2.7 Schematic representation of DSSC (Nogueira, Longo, and De Paoli 2004).

2.7.2 Dye sensitizer

Dye sensitizer serves as the solar energy absorber in DSSC. Its properties significantly affect the light harvesting efficiency and the overall photovoltaic conversion efficiency. Three dyes can be considered as the backbone of applied sensitizers in DSSC. All of these dyes are ruthenium-based metal-organic complexes with the general formula $\text{RuLxL}'\text{ySCNz}$, where L and L' are polypyridyl ligands. Nowadays, they are readily commercialized with excellent overall photovoltaic conversion efficiency up to 11% (Lenzmann and Kroon 2007). The molecular structure of these dyes is shown in Figure 2.8. Because of the complex chemical nomenclature, they are most often referred to trivial names as N-3 and N-719 for red and black dyes and Z-907. The N-3 dye is popular and it differs from N-719 dye in the degree of protonation. The black N-719 dye shows the broadest absorption range up to 900 nm. For Z-907 dye, its physicochemical properties are summarized in Table 2.2.

2.7.3 Electrolyte solution

The redox couple presented in the electrolyte is crucial important for stable operation of DSSC. The role of the electrolyte involves with the transportation of charges between the photoanode and the counter electrode during regeneration of the dye. After electron injection, the oxidized dye must be reduced to its ground state as fast as possible by the electron donor in the electrolyte. Thus, the choice of the charge mediator affects the electrolyte redox potential, which must be suitable for its efficient regeneration. In addition, the redox couple must be fully reversible and it should not absorb light in the same spectral region as the dye (Nogueira, Longo, and De Paoli 2004). The redox couple in the electrolyte influences the reduction of the oxidized state of the dye as well as the other processes in the DSSC, including electron transfer kinetics at the counter-electrode, dark current reactions, ion-pairing with the dye and also charge transportation in the semiconductor film and in solution (Oskam et al. 2001).

The electrolyte composition also affects the photovoltage (V_{oc}) of the DSSC, which is the difference between the Fermi level of the semiconductor and the electrochemical potential of the redox pair. Furthermore, the photovoltage can also be affected by non-electroactive species in the electrolyte, particularly by small cations such as protons, Li^+ , etc. These species can adsorb or intercalate onto the surface of the TiO_2 , shifting its conduction band edge to a lower energy level. The result may decrease the photovoltage, but they enhance the efficiency of interfacial charge injection, photocurrent and the overall efficiency of the DSSC (Kelly et al. 1999).

As previously mentioned for the electrolyte in DSSC, it is worthwhile to consider the sealing to prevent the loss of the liquid electrolyte by leakage and/or evaporation of the solvent. Thus, the injection of liquid electrolyte in DSSC requires a perfect seal

and binder having chemical resistance to the electrolyte (usually an organic solvent containing the corrosive I_3^-/I^- redox couple).

To consider the organic solvents used for preparation of electrolyte applied in DSSC, they have to decrease the viscosity of the electrolyte in order to promote the faster ion diffusion. The organic solvents generally used to prepare the liquid electrolyte are in the group of nitrile solvents such as acetonitrile, valeronitrile and 3-methoxypropionitrile.

2.7.4 Titanium dioxide or titania (TiO_2)

TiO_2 is one of n-type wide band gap semiconductor (band gap 3.2 eV) (Grätzel 2001) as shown in Figure 2.9. The TiO_2 has three main crystalline phases such as anatase showing the higher photocatalytic activity than other types of titania and it is suitable for DSSC, rutile having higher stability at high temperatures and brookite normally found only in minerals (Woodley and Catlow 2009). The titania phases are shown in Figure 2.10. Titania has many advantages in terms of low cost, wide availability, non-toxicity and biocompatibility. Thus, it can be applied for sensitized photochemistry and photo-electrochemistry (Grätzel 2003).

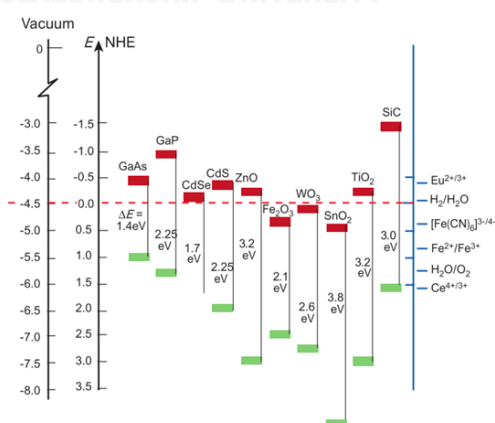


Figure 2.9 Band positions of several semiconductors in contact with aqueous electrolyte (red color = lower edge of the conduction band and green color = upper edge of the valence band) (Grätzel 2001).

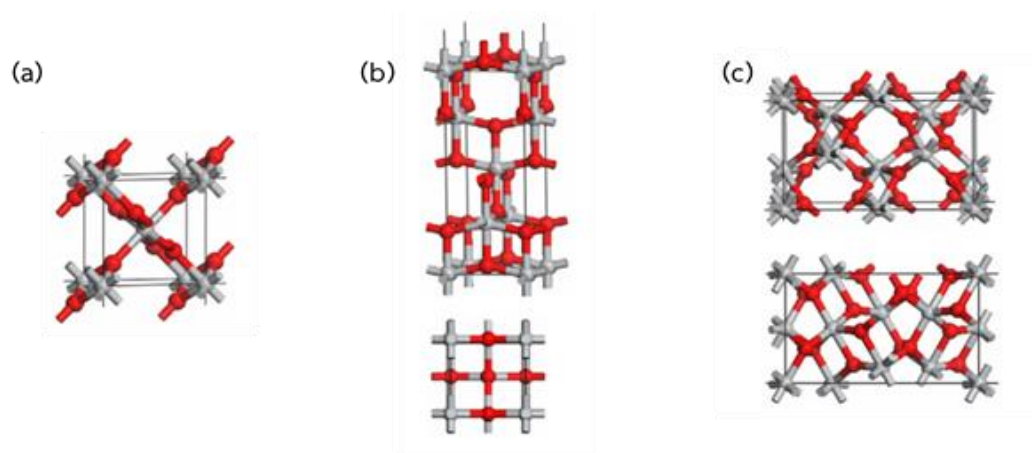


Figure 2.10 Titania phases (a) rutile, (b) anatase and (c) brookite (Woodley and Catlow 2009).

2.7.5 Counter electrode performance

The counter electrode (CE) is used to reduce the redox species, which act as a mediator in regenerating the sensitizer after electron injection in a liquid-state DSSC, or to collect holes from the hole transport material in a solid-state DSSC (Chen et al. 2010). Several kinds of catalytic materials for CE, such as platinum (Pt), carbon materials (graphite, activated carbon, carbon black and single-wall carbon nanotubes) (Imoto et al. 2003), PEDOT, polypyrrole and polyaniline have been introduced. Normally, Pt is used for this layer due to its high catalytic property affecting toward I₃⁻ reaction and superior chemical and electrochemical stabilities. A thin layer Pt nanoparticles is deposited onto FTO-glass by thermal deposition, sputtering or electrochemical deposition.

Thermal decomposition of H₂PtCl₆ dissolved in isopropanol solution is widely used to prepare high performance Pt-CE, because it is stable and shows higher exchange current density for the I₃⁻/I⁻ couple (Murakami and Grätzel 2008). However, this process requires a heat treatment with high temperature (>390 °C).

2.8 Operating principles of DSSC

In more detail, the different steps of the photoconversion process can be described in conjunction with the energy band diagram and the schematic structure of DSSC as shown in Figure 2.6. DSSC is consisted of substrates made from FTO-glass, a porous nanocrystalline semiconductor oxide (such as TiO_2) film sensitized by a dye (such as bipyridine ruthenium complexes) for absorbing visible light, a redox electrolyte layer (usually an organic solvent containing a redox system, such as I^-/I_3^- couple) for deoxidizing oxidized dye, and a Pt-cathode to collect electrons and catalyze the redox couple regeneration (O'Regan and Grätzel 1991). The light-to-electricity conversion in a DSSC is based on the injection of electron from the photoexcited state of the sensitized dye into the conduction band of TiO_2 . The dye is regenerated by electron donation from iodide in the electrolyte. The iodide is restored by the reduction of I_3^- at the cathode with the completion of circuit via electron migration through the external load. The voltage generated under illumination corresponds to the difference between the Fermi level of the electron in the TiO_2 and the redox potential of the electrolyte. Overall, the device generates electric power from light without suffering any permanent chemical transformation (O'Regan and Grätzel 1991; Grätzel 2001; Haque et al. 2005).

The photoelectric chemical process in DSSC can be expressed as Eq. 2.1–2.6. The photoexcited electron injects into the conduction band of TiO_2 (Hagfeldt and Grätzel 1995; Benko et al. 2002). The dark reactions (Eq. 2.5 and 2.6) also occur during the light-to-electricity conversion, but they do not play a remarkable negative effect on photovoltaic performance of DSSCs owing to their slow reaction speed compared with that of Eq. 2.2 (Asbury et al. 2001; Stier, Duncan, and Prezhdo 2004).



It can be seen that DSSC are a kind of complex system for light-to-electricity conversion. As a basic component, the electrolyte plays an important role in the process of light-to-electricity conversion in DSSC. The electrolytes employed in DSSC can be classified as liquid, solid-state, or quasi-solidstate. Several aspects are essential for any electrolytes in a DSSC as follows (Nogueira, Longo, and De Paoli 2004; Li et al. 2006):

(1) The electrolyte must be able to transport the charge carrier between photoanode and counter electrode. After injection of electrons produced by dye into the conduction band of TiO_2 , the oxidized dye must be rapidly reduced to its ground state. Thus, the electrolyte should promote the dye redox potential and regeneration of itself.

(2) The electrolyte has to provide the fast diffusion of charge carriers (higher conductivity) and produce good interfacial contact with the porous nanocrystalline layer and the counter electrode. For liquid electrolytes, it is necessary to prevent the loss of the liquid electrolyte by leakage and/or evaporation of solvent.

(3) The electrolyte must have long-term stability, including chemical, thermal, optical, electrochemical, and interfacial stability. Moreover, it does not cause the desorption and degradation of the dye from the oxide surface.

(4) The electrolyte should not exhibit a significant absorption in the range of visible light. For the electrolyte containing I^-/I_3^- redox couple, I_3^- shows color and dye can reduce the visible light absorption of electrolyte. I_3^- ions can react with the injected electrons and increase the dark current. Thus, the concentration of I^-/I_3^- must be optimized.

2.9 Literature reviews

The following previous literatures indicate the conducting polymers, which are suitable materials for replacing the Pt-counter electrode in DSSC. Some counter electrodes made from plastic substrates, which are modified to enhance the electrical conductivity by coating with conductive polymers via spin coating, sputtering and print screen techniques.

Saito et al. (2004) studied the effect of *p*-toluenesulfonate doped PEDOT (PEDOT-TsO) thickness on I_3^-/I^- redox reaction behavior, and the charge transfer resistance between PEDOT-TsO and Pt counter electrodes and the I_3^-/I^- redox couple. The performance of these counter electrodes was also evaluated by photovoltaic characteristics of the DSSC. The preparation methods of these counter electrodes are attractive. PEDOT-TsO was produced by chemical polymerization of the monomer 3,4- ethylenedioxythiophene catalyzed by Fe(III) tris-*p*-toluenesulfonate. The two components were spin-coated together and then heated at 110 °C for 5 min for polymerization. After polymerization, the samples were rinsed by using methanol to remove the Fe(II) bis-*p*-toluenesulfonate from the film and dried. The results showed that I_3^-/I^- redox reaction on PEDOT-TsO electrode was similar to that sputtered Pt electrode. The charge transfer resistance (R_{CT}) on the interface of electrolyte/PEDOT-

TsO decreased with increasing the thickness of PEDOT-TsO layer. It was found that the cell with thicker PEDOT-TsO counter electrodes (thickness $\sim 2 \mu\text{m}$) showed higher open-circuit voltage (V_{OC}), fill factor (FF), and total conversion efficiency than the cell with PEDOT-TsO counter electrodes having $\sim 50 \text{ nm}$ thickness and Pt counter electrodes (thickness $\sim 70 \text{ nm}$) when ionic liquid was used as the electrolyte.

Garganourakis et al. (2009) studied the influence of ZnO film thickness grown on flexible poly(ethylene terephthalate) (PET) substrate on its optical and surface properties for applying as transparent conductive oxides (TCOs) in flexible electronic devices (FEDs). PEDOT:PSS thin films were spin-coated onto ZnO/PET substrates and their properties were investigated in relation with the ZnO thickness controlled by the deposition time. When the thickness of ZnO films increased, the surface roughness of the ZnO films increased. However, the ZnO thickness does not affect the energy gap (E_g) values. The surface roughness of the ZnO films increased, but after the thickness of ZnO 350 nm no further increasing roughness was observed. The ZnO films thickness affected the properties of PEDOT:PSS films. The high surface roughness of ZnO film induced a high amount of PEDOT:PSS molecules seep through the ZnO columns leading the thicker interface layer and thinner PEDOT:PSS layer. However, the optical properties of PEDOT:PSS were almost constant with respect to the ZnO thickness. These results were valuable for the development of p-n junction materials for application in the flexible optoelectronic devices such as organic light emitting diodes (OLEDs) technology and organic photovoltaics (OPVs).

Chen et al. (2010) attempted to fabricate Pt counter electrodes on the flexible indium-doped tin oxide coated polyethylene naphthalate (ITO-PEN) substrates by screen printing technique followed by chemical reduction method. The common pressure hydrothermal method was used as a post-treatment for Pt counter electrode at low temperature. This step took place in a non-sealed at $100 \text{ }^\circ\text{C}$ at common pressure. They screen chloroplatinic acid hexahydrate ($\text{H}_2\text{PtCl}_6 \cdot 6\text{H}_2\text{O}$) in terpineol

solution on ITO-PEN substrates ($\text{H}_2\text{PtCl}_6/\text{ITO-PEN}$) followed by reducing Pt^{4+} in sodium borohydride (NaBH_4) solution and rinsed with distilled water. Then, $\text{H}_2\text{PtCl}_6/\text{ITO-PEN}$ counter electrode was post-treatment. This technique was convenient and cheap and it could be used for the flexible polymer substrates. The results showed that the conversion efficiency of the flexible DSSC increased with increasing the H_2PtCl_6 concentration and reached to a maximum value at 0.6 wt%. Above this point, the conversion efficiency decreased with the concentration. Based on these photovoltaic parameter, the conversion efficiency enhancement is attributable to the promotion of the short-circuit current (J_{sc}) and FF. It was found that the flexible DSSC fabricated by the Pt counter electrode prepared with the 0.6 wt% $\text{H}_2\text{PtCl}_6 \cdot 6\text{H}_2\text{O}$ terpineol solution (hydrothermal treatment) gave the highest electricity conversion efficiency of 5.41%. The flexible DSSC based on the prepared counter electrode without the hydrothermal treatment showed lower FF and conversion efficiency. It was known that FF was strongly depended on the internal resistance of the cell. A higher FF was obtained for the cell based on Pt counter electrodes with the lower resistance of charge transfer (R_{CT}) on the electrolyte/Pt interface. The satisfied photovoltaic performance of the prepared Pt counter electrodes was attributed to the hydrothermal treatment, in which process the organic residues was removed, and thus R_{CT} of the prepared Pt counter electrode was decreased.

Wang, Wei and Hu (2013) investigated the effect of ZnO used as the counter electrode on the DSSC performance. ZnO was expected to have a strong interaction with the ions of iodine-based electrolytes leading the excellent catalytic activity. However, ZnO had poor electrical conductivity. Thus, it is necessary to combine ZnO with a conductive component such as PEDOT:PSS. PEDOT was not only used as a conductive polymer, but it also acted as a catalyst for I_3^-/I^- redox reaction in DSSC. It was found that the combination of ZnO and PEDOT used as the counter electrode for DSSC exhibited the maximum total conversion efficiency as 8.17% since the interaction

energy of I_3^- and ZnO (30 kcal/mol) was higher than that of I_3^- and only PEDOT (8.4 kcal/mol) for I_3^- reduction. Thus, the integration of ZnO and PEDOT had potential to replace the expensive Pt catalyst generally used as the catalyst for I_3^- reduction in the DSSC.

Sahito et al (2016) presented a highly conductive-graphene coated cotton fabric (HC-GCH) used as the counter electrode for DSSC. This novel flexible counter electrode was not only cheaper than Pt, but it also require low temperature treatment. This electrode could be easily prepared in bulk using a simple, dip and dry technique followed by chemical reduction. The results showed that the DSSC based on Pt-FTO provided 8.44% total conversion efficiency with FF of 0.79, V_{OC} of 0.67 V and J_{SC} of 15.88 mA/cm²; whereas, the HC-GCF counter electrode-cells showed the total conversion efficiency as 6.93%, with FF of 0.71, V_{OC} of 0.66 V and J_{SC} of 14.75 mA/cm². This indicated that, the HC-GCF reached 82.11% of total conversion efficiency provided by Pt-FTO electrode. The slightly lower J_{SC} of 14.75 mA/cm² and a minor decrease in V_{OC} value might be due to the higher R_{CT} of the HC-GCF counter electrode. Because of the geometry of the fabric, it might provide better microporous structure compared to the Pt, yet the filmness of the fabric was inferior when it was compared to the Pt-FTO electrode. According to the low temperature preparation of the proposed counter electrode providing the its cost effectiveness, flexibility and organic nature, HC-GCF could be considered as an innovative and stable counter electrode for various applications. Therefore, it was believed, that the HC-GCF electrode would be considered as a strong candidate to replace Pt in future for the further development of low cost, flexible and efficient solar cells.

CHAPTER III

EXPERIMENTAL

3.1 Materials and chemicals

3,4-Ethylenedioxythiophene (EDOT) monomer, Fe (III) p-toluene sulfonate hexahydrate ($\text{Fe}_2(\text{SO}_4)_3 \cdot 6\text{H}_2\text{O}$), anisole, lithium hydroxide monohydrate ($\text{LiOH} \cdot \text{H}_2\text{O}$), 3-(trimethoxysilyl)propyl methacrylate (TPM), ethanol, butanol, lithium perchlorate (LiClO_4) and 2-methylimidazole were purchased from Sigma-Aldrich (USA). Chloroform (CHCl_3) and iodine (I_2) were purchased from Quality Reagent Chemical (New Zealand). Tert-butyl Alcohol from Panreac (Spain), acetonitrile from Labscan (Thailand), zinc acetate ($\text{Zn}(\text{CH}_3\text{COO})_2 \cdot 2\text{H}_2\text{O}$) from Ajax Finechem Pty. Ltd. (Australia), lithium iodide (LiI) from ACROS organics (USA) and pyridine from Merck (Germany) were analytical grade and used as received. PMMA sheets ($20 \times 20 \times 2 \text{ mm}^3$) with $10^{14} \Omega/\text{cm}^2$ electrical resistance were purchased from Ying Yong Plastic Glass Co., Ltd. (Thailand). The granulous PMMA was provided by IRPC Public Co., Ltd (Thailand). The $20 \times 20 \times 2 \text{ mm}^3$ FTO conductive glass (electrical resistance (R_{sh}) = $20 \Omega/\text{cm}^2$) is purchased from Xin Yan Tech (Hong Kong), transparent titania paste (TiO_2) having average particle size of 20 nm and *cis*-bis(isothiocyanato) (2,2'-bipyridyl-4,4'-dicarboxylato) (4,4'-di-nonyl-2'-bipyridyl)ruthenium(II) (Z907) hydrophobic dye were obtained from Dyesol (Australia). Iodolyte HI-30 electrolyte, surlyn (60 μm) were purchased from Solaronix (Switzerland). Hexachloroplatinic (IV) acid (PtCl_6^{2-}) and titanium (IV) chloride (TiCl_4) were received from Merck (Germany). Silver/Silver Chloride (Ag/AgCl) reference electrode was purchased from Metrohm (Germany).

3.2 Preparation of PEDOT/PMMA sheets

The poly(3,4-ethylenedioxythiophene) (PEDOT) was deposited onto the PMMA sheet via *in situ* polymerization of 0.1-0.4 mL EDOT (0.24 M) dissolved in ultra-pure water containing Fe (III) p-toluene sulfonate in butanol (0.45 M) and pyridine (0.22 M) (Hansen et al. 2006). This solution was then applied onto the surface of PMMA sheet using spin coating technique with the spinning rate of 300-1,000 rpm for 15-60 s. The obtained substrate was then heated at 65°C for 10 min on a hotplate to evaporate the remaining solvent and initiate the polymerization to produce PEDOT/PMMA sheets. After washing by 1 mL butanol/anisole mixture (1/1 (v/v)) under the spinning rate at 1,000 rpm for 20 s, the PEDOT/PMMA sheet was further dried at 65°C on the hotplate for 5 min. The 20 μ L 2-methylimidazole in ethanol (2-methylimidazole solution/EDOT = 1/10 (w/w)) was gradually dropped throughout the surface of the PEDOT/PMMA sheets. The polymeric films were subsequently annealed on a hot plate at 130 °C for 30 min and then at 230 °C for 1 min. The standard condition used for coating PEDOT on PMMA sheet is summarized in Table 3.1.

Table 3.1 Recipe for preparation of PEDOT/PMMA sheets.

Parameters	Condition
Concentration of EDOT monomer (M)	0.1-0.7
Spinning rate (rpm)	300-1000
Spinning time (s)	15-60
Reaction temperature (°C)	65
Concentration of 2-methylimidazole in ethanol (M)	1-6

3.3 Preparation of PEDOT/ZnO/PMMA sheets

The ZnO layer on the PMMA substrate was prepared via sol-gel technique as described in the previous work (Zhang et al. 2013). Briefly, the solution of $\text{Zn}(\text{CH}_3\text{COO})_2 \cdot 2\text{H}_2\text{O}$ (2.2 mmol) and $\text{LiOH} \cdot \text{H}_2\text{O}$ (8.6 mmol) in ethanol (100 mL) was stirred at 70 °C for 2 h to produce well-dispersed ZnO particles (77.59 g/batch). Then, TPM (25 μL) used as the coupling agent between ZnO and PMMA phases and distilled water (100 μL) were added into the above solution. The obtained mixture was placed in the ultrasonic bath (NXPC 1505 (P), Korea) for 10 min and then magnetically stirred for 2 h at room temperature. The obtained ZnO solution (1-5 mL) was added into the PMMA syrup which was prepared by dissolving PMMA granules (1.85 g) in 10 mL CHCl_3 . After stirring for 15 min, the mixture was applied on the surface of the PMMA sheet using the spin coating (Autolab, Netherland) at 3,000 rpm for 30 s to produce the ZnO layer (600 μL) on the PMMA sheet (ZnO/PMMA). The deposition of PEDOT onto the ZnO/PMMA sheets were then carried out following the direction of PEDOT/PMMA sheets preparation as described in the section of 3.2 to obtain the PEDOT/ZnO/PMMA sheets.

The PEDOT/ZnO/PMMA sheet was further dried at 65°C on the hotplate for 5 min. The 2-methylimidazole in ethanol solution (5 M) (2-methylimidazole solution/EDOT = 1/10 (w/w)) was gradually dropped throughout the surface of PEDOT/ZnO/PMMA sheet. The polymeric films were subsequently annealed on a hot plate at 130 °C for 30 min and then at 230 °C for 1 min.

3.4 Fabrication of DSSC

To prepare DSSC photoanode, the FTO glass surface was treated by immersing in the 0.04 M TiCl_4 solution for 30 min at 60°C. Then, TiO_2 paste was screen-printed on treated FTO glass for 3 times (0.01 g TiO_2 paste/time) using a block screen with mesh

size of 90T. The obtained TiO_2 -coated FTO glass was successively sintered at 325 °C for 5 min, 375 °C for 5 min, 450 °C for 15 min and 500 °C for 15 min. The final thickness of TiO_2 layer on the FTO glass was ca. 9 μm . After cooled down to ~ 80 °C, TiO_2 -coated FTO glass was dipped into 0.3 mM Z907 dye solution using acetonitrile/tert-butyl alcohol (1/1 (v/v)) as solvent mixture for 18 h.

For the counter electrode (cathode side), the modified PMMA sheet, PEDOT/PMMA or PEDOT/ZnO/PMMA sheets, was drilled to make a hole for liquid electrolyte injection. The two electrodes were assembled by hot-press at 120 °C using 60 μm surlyn ring as a spacer. The liquid electrolyte (I_3^-/I^- redox) was injected through the hole on the modified PMMA sheet and then the hole was sealed by a cover glass ($9 \times 9 \text{ mm}^2$ with 0.13-0.17 mm thickness). The active area of the fabricated DSSC was 0.25 cm^2 . The detail of DSSC fabrication is illustrated in Figure 3.1. The cross-sectional DSSC cell is shown in Figure 3.2.

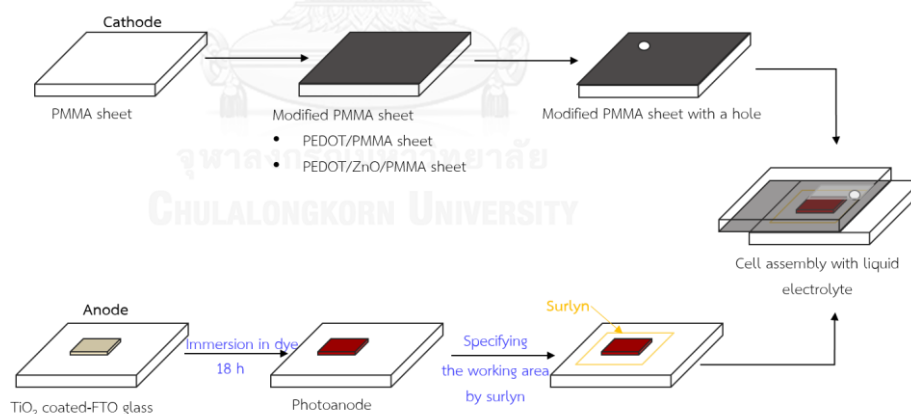


Figure 3.1 Schematic diagram of DSSC preparation using the modified PMMA sheet acting as the counter electrode.

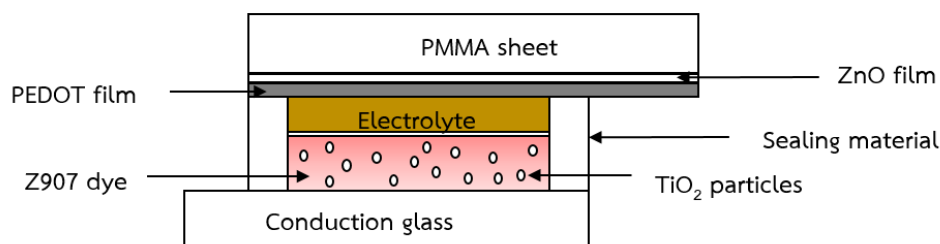


Figure 3.2 Cross-section of assembled DSSC module.

3.5 Characteristic and physical properties of the modified PMMA sheets

3.5.1 Structural characterization of PEDOT film on the modified PMMA sheets

The chemical structure of PEDOT film coated on the modified PMMA sheets were analyzed by using an attenuated total reflectance Fourier transform infrared (ATR-FTIR, Perkin Elmer, spectrometer (USA)). All samples were carried out at room temperature over the wavenumber range of 500-4,000 cm^{-1} with 64 scan in 0.5 cm^{-1} resolution.

3.5.2 Type and crystalline matter on PEDOT/ZnO/PMMA sheets

The existence of ZnO on the PEDOT/ZnO/PMMA sheets was detected by using X-ray diffractometry (XRD; Bruker D8 advance XRD system) operated at 40 kV and 40 mA with Cu-K α radiation source ($\lambda = 1.54 \text{ \AA}$). The measurement range is $2\theta = 10-80^\circ$ with the degree changing rate of 0.1 $^\circ$ /s.

3.5.3 Morphology and topology of the modified PMMA sheets

The morphology image of ZnO/PMMA sheets were observed with energy dispersive X-ray spectroscopy (EDS) (Model 7573) (15 kV) and the thickness of PEDOT or ZnO layers were measured by using scanning electron

microscopy (SEM; JEOL Model JSM6480LV) operated at 15 kV. Before analysis, the samples were sputter-coated with gold in order to increase the conductivity.

The topology of the surface of modified PMMA sheets was detected by using atomic force microscopy (AFM; Asylum research) equipped with a scanning probe microscope and a NanoScope III controller. The measurement was operated in the tapping mode with a 50 N.m^{-1} probe and a scan rate of 170 kHz under ambient condition.

3.5.4 Contact angle of surlyn and modified PMMA sheets

The water contact angles of the surlyn, 2-methylimidazole/PEDOT/ZnO/PMMA sheet and PEDOT/ZnO/PMMA sheet were measured by using a microscope equipped with a Kruss (DSA 10 MK2, Germany) at room temperature. The injection volume of deionized water was controlled as 0.5 μL .

3.5.5 Electrical resistivity and conductivity of the modified PMMA sheets

The electrical resistivity (R) of the modified PMMA sheets was detected by using the standard four-point probe (RM3-AR JENDEL) as shown in Figure 3.3a. If the sample has any resistance to the flow of electrical current, the potential (or voltage) as the current flows will be dropped along the sample. From Figure 3.3b, the drop of voltage generated between probes (at the label 2 and 3) could be measured by a digital voltmeter. This resistance between probes 2 and 3 was the ratio of the voltage registering on the digital voltmeter to the value of the output electrical conductivity (σ) of the power supply. The high impedance of the digital voltmeter minimized the current flow through

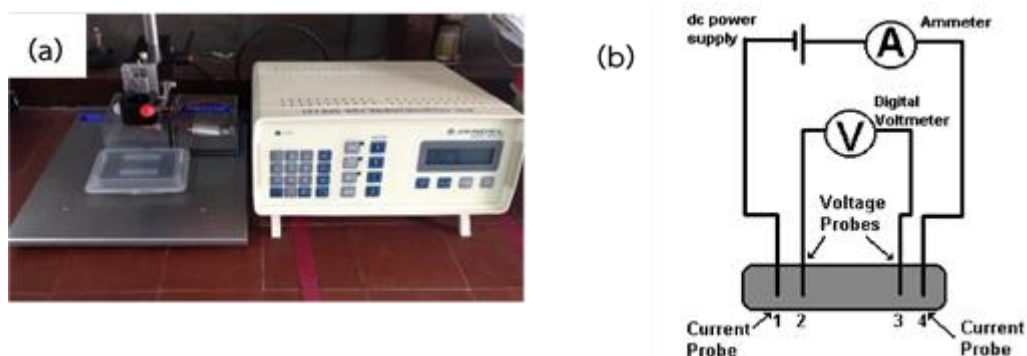


Figure 3.3 Four-point probe conductivity cell.

the portion of the circuit comprising the voltmeter. Thus, there was no potential drop across the contact resistance associated with probes 2 and 3. Only the resistance associated with the superconductor between probes 2 and 3 was measured. The electrical conductivity (σ (S/cm)) of the surface of each specimens was then calculated from Eq. 3.1 (Kim et al. 2010).

$$\rho = R_s \times t \quad (3.1)$$

$$\sigma = \frac{1}{\rho} \quad (3.2)$$

where t is the sample thickness (cm) of the PEDOT layer on the modified PMMA sheets, ρ is the electrical resistivity ($\Omega \cdot \text{cm}$) of the specimens and R_s is the sheet resistance (Ω/cm^2).

3.5.6 Catalytic activity of PEDOT for I_3^-/I^- redox

The activity of PEDOT for catalyzing I_3^-/I^- redox reaction was tested by using cyclic voltammograms (CVs) technique. In general, this technique is performed in acetonitrile solution. However, PMMA sheet could not stand in this solution. To avoid this problem, 0.22 mL EDOT solution in ultra-pure water (0.24 M) was instead coated on the FTO glass or ZnO/FTO glass prepared from 3 mL ZnO colloidal solution. The cyclic voltammetry measurement was

consisted of 3 electrodes (PEDOT/FTO glass or PEDOT/ZnO/FTO glass used as the working electrode; Pt wire used as the counter electrode and Ag/AgCl used as a reference electrode) in the presence of acetonitrile solution (200 mL) containing 10 mM LiI, 1 mM I₂ and 0.1 M LiClO₄.

3.6 Electrochemical properties of DSSC

The current voltage measurement (I-V test) was used to evaluate the electrochemical properties of DSSC test devices. The I-V characteristics was measured under illumination of ELH (1 sun to equivalent to 100 mW/cm² (AM 1.5)) from solar simulator in an ambient atmosphere. The profile of voltage vs. current density (I-V curve) was observed as shown in Figure 3.4. The detail of fill factor (FF) and cell resistance were then calculated from I-V curve following Eq. 3.3.

$$FF = \frac{P_{max}}{V_{oc} \times I_{sc}} = \frac{V_{max} \times I_{max}}{V_{oc} \times J_{sc}} \quad (3.3)$$

Finally, the energy conversion efficiency (η) was also obtained from Eq. 3.4 (Xiao et al. 2012).

$$\eta = \frac{P_{max}}{P_{light}} \times 100\% = \frac{V_{oc} \times J_{sc} \times FF}{P_{light}} \times 100\% \quad (3.4)$$

where J_{sc} is the short-circuit current density (mA/cm²), V_{oc} is the open-circuit voltage (V), P_{light} is the incident light power, J_{max} (mA/cm²) and V_{max} (V) are the current density and the voltage at the point of maximum power output in the J - V curves, respectively (as shown is Figure 3.4).

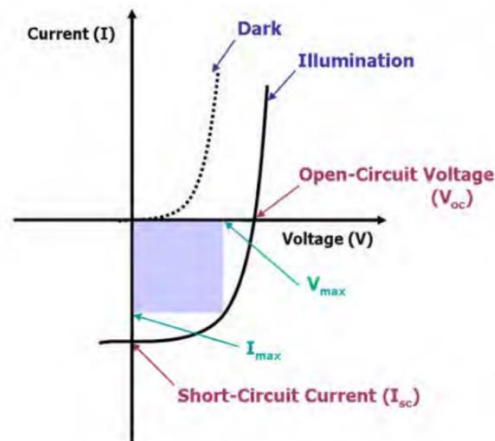


Figure 3.4 I-V characteristic of an illuminated solarcell (Kim et al. 2011).

The incident monochromatic photon-to-current conversion efficiencies (IPCE) of the DSSC device under short-circuit condition were measured with an Oriel 150W Xenon (Xe) lamp fitted with a Cornerstone™ 130 1/8 m monochromator used as a monochromatic light source, a Newport 818-UV silicon photodiode used as the power density calibration and a Keithley 6485 picoammeter. All measurements were performed by using a black plastic mask with an aperture area of 0.180 cm² and no mismatch correction for the efficiency conversion data. IPCE was calculated according to the following Eq. 3.5 (Susmitha et al. 2015).

$$\text{IPCE} = \frac{1240 \text{ (eV nm)} \times J_{\text{sc}} \text{ (mA/cm}^2\text{)}}{\lambda \text{ (nm)} \times \phi \text{ (mW/cm}^2\text{)}} \quad (3.5)$$

where J_{sc} is the short-circuit photocurrent density for monochromatic irradiation, λ and ϕ are the wavelength and the intensity, respectively, of the monochromatic light.

CHAPTER IV

RESULTS AND DISCUSSIONS

This research could be device as 2 part. For the first part, it involved with the preparation of the conductive poly(methyl methacrylate) (PMMA) sheets via spin coating of 3,4-ethylenedioxythiophene (EDOT) monomer. The effect of EDOT concentration and 2-methylimidazole content on the poly(3,4-ethylenedioxythiophene) (PEDOT) film thickness on the electrical resistivity and topology of the modified PMMA was studied with or without the addition of zinc oxide (ZnO) layer. The second part was related to the study of the possibility to replace the counter electrode in the dye-sensitized solar (DSSC) by using the PEDOT/PMMA or PEDOT/ZnO/PMMA sheets. The overall energy efficiency of the DSSC having the modified PMMA sheets was comparatively evaluated.

4.1 Structural characterization of PEDOT deposited on the modified PMMA sheets

The ATR-FTIR spectrum of PEDOT deposited on the modified PMMA sheets was shown in Figure 4.1 and compared to PEDOT powder. The main characteristic peak of the PEDOT powder showed at approximately 1,630-1,648 cm^{-1} , which was attributed to the C=C stretching of thiophene. The characteristic signals of C-O-C bond stretching in the ethylene dioxy group of PEDOT were also found at 1,174, 1,186 and 1,139 cm^{-1} . Moreover, the peaks of C-S bond in the thiophene ring were observed at 977, 810 and 682 cm^{-1} . To compare with the ATR-FTIR spectrum of PEDOT film coated on the surface of PMMA, the similar characteristic peaks to the PEDOT structure were observe as mentioned above. Thus, this indicated the success of coating PEDOT onto the PMMA surface.

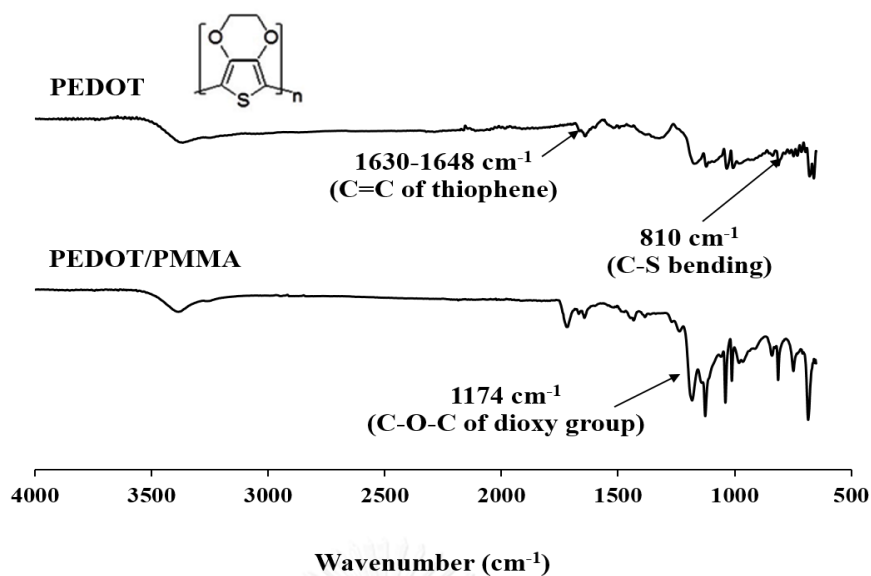


Figure 4.1 ATR-FTIR spectrum of the PEDOT deposited on the PMMA sheet compared to that of PEDOT powder.

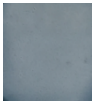




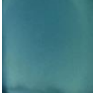
4.2 Initial study of suitable EDOT monomer concentration and spinning time for preparation of modified PMMA sheets

Normally, FTO glass used in DSSC or electrical device has the electrical resistance only $20 \Omega/\text{cm}^2$. However, PMMA sheet is the non-conductive material with high electrical resistance as $10^{14} \Omega/\text{cm}^2$. Therefore, it can't be directly applied into those devices. To enhance the conductivity of PMMA sheets, the suitable EDOT concentration and spinning time were initially evaluated for preparation of the conductive PMMA sheets. Thus, the objective of this section was to investigate the suitable EDOT monomer concentration and the spinning time for coating EDOT monomer on electrical resistance and appearance of the modified PMMA sheets. The volume of EDOT solution in the presence of butanol was kept constant at $150 \mu\text{L}$ using 300 rpm spinning rate. The result were summarized in Table 4.1. For the different EDOT monomer concentrations, it was found that the increasing EDOT concentration decreased the electrical resistance of the modified PMMA sheets due to the higher

PEDOT content obtained from the *in situ* polymerization of applied EDOT monomer. Although the use of EDOT concentration at 0.72 M provided the modified PMMA sheets with the lowest electrical resistance as $21.18 \Omega/\text{cm}^2$, this point was not significantly different from the use of EDOT concentration at 0.24 M. Moreover, the use of high EDOT concentration provided the darker modified PMMA sheets.

For the effect of spinning time, the increase in the spinning time from 15 to 60 s increased the electrical resistance from 28 to $110 \Omega/\text{cm}^2$. This could be explained that some portion of EDOT solution was ejected from the surface of PMMA sheets with longer spinning time. The phenomenon could be shown by the reduction of the PEDOT color of the modified PMMA sheets. Thus, the EDOT concentration at 0.24 M with spinning time of 30 s was appropriate condition for further study.

Table 4.1 Effect of EDOT monomer content and spinning time on electrical resistance and appearance of the modified PMMA sheets

Concentration of EDOT monomer (M)	Spinning time (s)	Electrical resistance (Ω/cm^2)	Sheets appearance
0.12	30	119.4 ± 1.66	
0.24	30	30.65 ± 1.39	
0.72	30	21.18 ± 1.45	
0.24	15	27.99 ± 1.54	
0.24	45	34.10 ± 0.52	
0.24	60	110.6 ± 6.92	

^a EDOT was dissolve in butanol and EDOT solution (150 μL) was spinned at 300 rpm.

4.3 Effect of spinning rate, number of EDOT layers and 2-methylimidazole content on electrical resistance and appearance of modified PMMA sheets

The effect of the spinning rate for coating EDOT solution on PEDOT film thickness, electrical resistance and appearance of the PEDOT/PMMA sheets was evaluated. Figure 4.2 showed that the increase in the spinning rate from 300 to 1,000 rpm for 30 s decreased the PEDOT film thickness on the surface of the modified PMMA sheets from 2.3 to 1.3 μm due to the higher ejection volume of EDOT solution during rotation (Krebs 2009). This could be seen from the pale color of PEDOT film reflecting the less PEDOT content on the PMMA surface (Table 4.2). This consequently resulted the reduction of electrical resistance from 30 to 2,020 Ω/cm^2 as shown in Table 4.2.

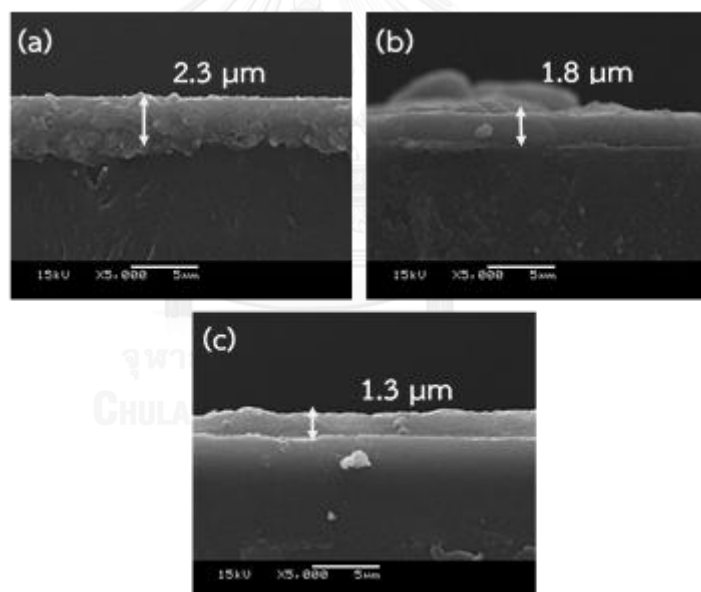

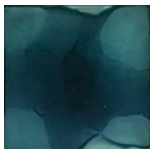
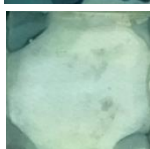


Figure 4.2 SEM images of the cross-section of PEDOT film on PMMA sheet obtained from various spinning rates: (a) 300 rpm, (b) 500 rpm and (c) 1,000 rpm.

Table 4.2 Effect of spinning rate on PEDOT film thickness and electrical resistance and appearance of PEDOT/PMMA sheets





Spinning rate (rpm)	Thickness (μm)	Electrical resistance (Ω/cm^2)	Appearance
300	2.3	30.65 ± 1.39	
500	1.8	131.6 ± 5.17	
1000	1.3	$2,020 \pm 127$	

*Condition: EDOT monomer = 0.24 M, spinning time = 30 s.

From the Section 4.3, the effect of PEDOT layer and the addition of 2-methylimidazole on the reduction of electrical resistance and appearance of the modified PMMA sheets were also studied as shown in Table 4.3. It was found that the increase in the PEDOT layers from 1 to 3 layers provided the higher non-homogeneity of the PEDOT film resulted in the higher electrical resistance from 30 to 91 Ω/cm^2 .

From the previous literature (Saghaei, Fallahzadeh, and Yousefi 2015), it was reported that the post treatment with the 2-methylimidazole solution in ethanol could enhance the electrical conductivity of PEDOT: poly(styrene sulfonate) (PSS) film from 0.8 to 930 S/cm. For this research, the results in Table 4.3 exhibited that the increase in the concentration of 2-methylimidazole to 5 M could decrease the electrical resistance to 12 Ω/cm^2 , which was lower than that of FTO glass (20 Ω/cm^2). However, the over concentration of 2-methylimidazole above 6 M increase the electrical resistance to 61 Ω/cm^2 possibly due to the high viscosity of 2-methylimidazole solution providing the difficult distribution throughout the PMMA sheets.

Table 4.3 Effect of number of PEDOT layers and 2-methylimidazole content on electrical conductivity of modified PMMA sheets

Number of PEDOT layers	Concentration of 2-methylimidazole (M)	Electrical resistance (Ω/cm^2)	Sheets appearance
1	-	30.65 ± 1.39	
2	-	86.78 ± 0.08	
3	-	91.80 ± 0.14	
1	0	30.65 ± 1.39	
1	1	33.26 ± 0.02	
1	3	19.30 ± 0.13	
1	5	12.20 ± 0.18	
1	6	61.60 ± 2.14	

*Condition: EDOT concentration = 0.24 M, spinning time = 30 s, spinning rate = 300 rpm

4.4 Effect of zinc oxide layer on the properties of modified PMMA sheets

To enhance the electrical conductivity of PEDOT, Hu et al (2013) reported that the incorporation of PEDOT with ZnO increased the energy conversion efficiency of electrical device such as DSSC from 4.6% to 8.17% depended on the amount of ZnO. Thus, this research attempted to add ZnO layer onto the PMMA sheets via spin coating technique at 3,000 rpm for 30 s before coating with EDOT solution (0.24 M) using the

same technique at 300 rpm for 30 s. Before spin coating, the ZnO colloidal prepared from the Section 3.3 (77.59 g ZnO/100 mL ethanol) was mixed with the PMMA syrup (1.85 g PMMA resin in 10 mL chloroform). The ZnO concentration in the PMMA syrup was varied in the rang of 10-58 wt%. The crystalline size of ZnO in the obtained colloid, the amount of ZnO on the modified PMMA sheet, the morphology and electrical resistance of PEDOT/ZnO/PMMA sheets were examined and reported as shown below:

4.4.1 Crystalline structure of ZnO colloidal

Figure 4.3 shows the X-ray diffractometry (XRD pattern of ZnO powder. The XRD patterns of ZnO shows the diffraction peaks at 2θ of 31.8° , 34.6° , 36.4° , 47.8° , 56.8° , 63.1° , 68.2° , and 69.5° are associated to the (100), (002), (101), (102), (110), (103), (200), and (201) planes of the ZnO (Kulyk et al. 2010; Abdiryim et al. 2014). The average size of ZnO the particles could be calculated by the Debye-Scherrer formula as shown in Eq. 4.1:

$$D = \frac{0.9\lambda}{B \cos\theta_b} \quad (4.1)$$

where D is the average size of the particle, λ is the X-ray wavelength (1.54 \AA), B is the FWHM width of the diffraction peak, and θ_b is the corresponding diffraction angle of the diffraction peak. According to the data presented in Figure 4.3, the average particle size of the ZnO calculated from every crystalline plane was about 20 nm.

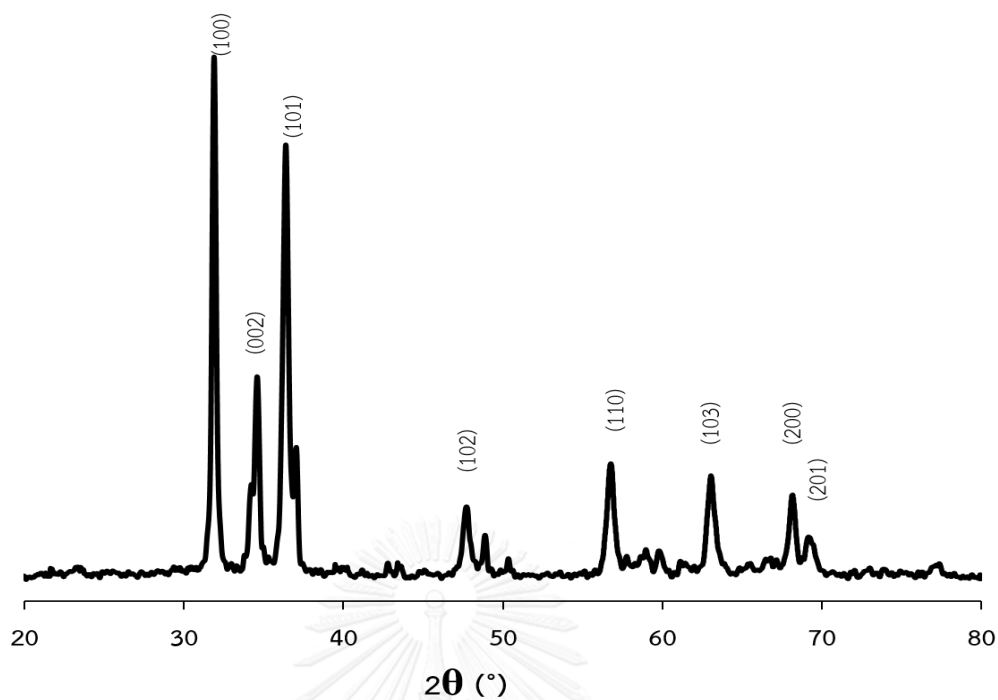


Figure 4.3 XRD pattern image of ZnO.

4.4.2 Energy dispersive X-ray spectroscopy (EDS) of ZnO/PMMA sheets

The EDS spectrum shown in Figure 4.4 indicated the spectrum of ZnO at 15 keV, which was similar to the previous observation (Zhang et al. 2011; Zhang et al. 2013). This result confirmed the combination of ZnO onto the surface of PMMA sheets. For the use of 10, 34, 58 wt% ZnO in the PMMA syrup, the ZnO content on the PMMA surface was 0.41%, 0.76% and 3.03%, respectively.

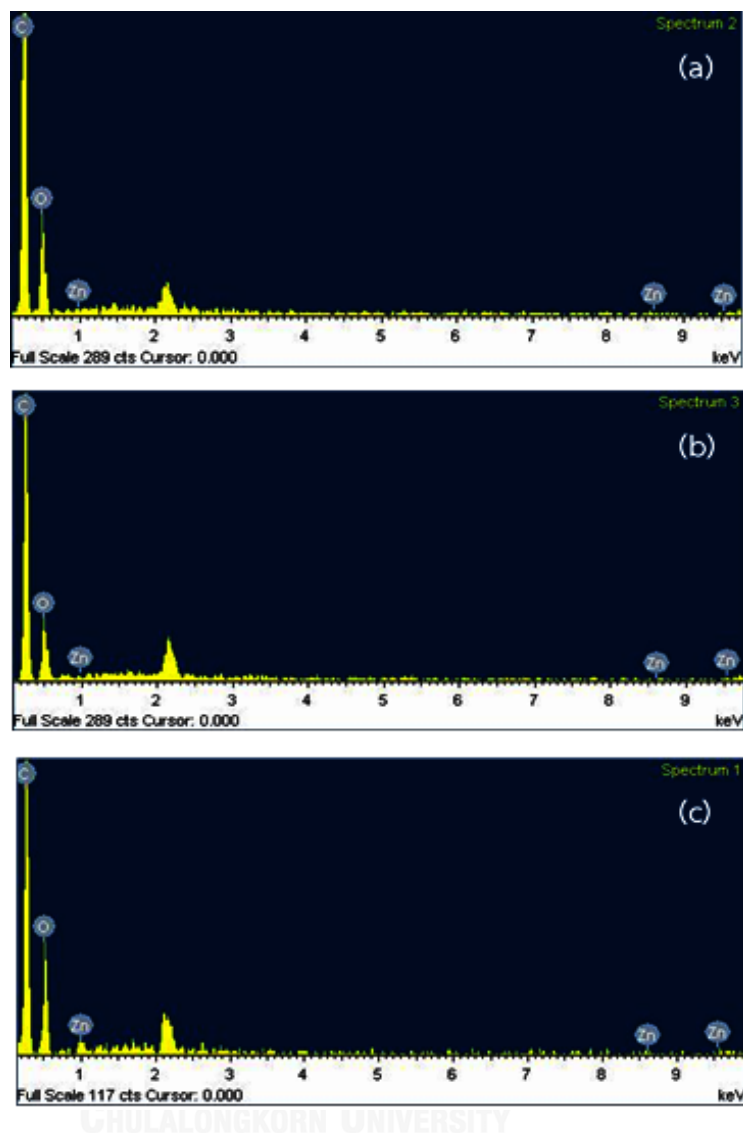


Figure 4.4 EDS spectrum of ZnO coated on the PMMA sheets: (a) 0.41, (b) 0.76 and (c) 3.03 wt% ZnO on PMMA sheets.

4.4.3 Morphology, topology and electrical resistance of PMMA/ZnO/PMMA sheets (modified PMMA sheets)

Figure 4.5 shows the cross-section area of the PEDOT/ZnO/PMMA sheets. The result indicated that the thickness of the ZnO layer covered on the PMMA surface was ca. 2.1 μm as shown in Figure 4.5a. After depositing EDOT solution (0.24 M) via

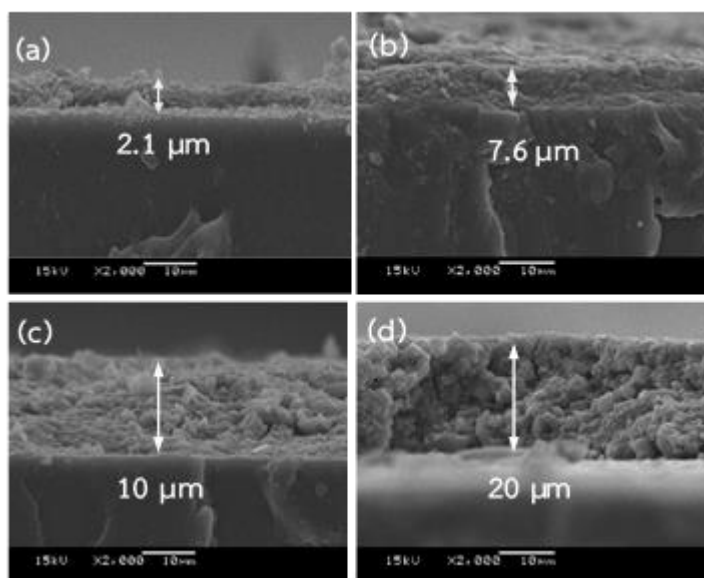


Figure 4.5 SEM images of the cross-section of the PEDOT/ZnO/PMMA sheets prepared by using various ZnO concentrations in the PMMA syrup: (a) 0 wt%, (b) 10 wt%, (c) 34 wt% and (d) 58 wt%.

spin coating onto the ZnO/PMMA sheet containing various ZnO content, the PEDOT layer could not be observed. It was possible that the EDOT solution was penetrated through the ZnO layer as illustrated in Figure 4.5b-4.5d (Garganourakis et al., 2009). This was due to the effect of roughness generated from the ZnO layer.

To evaluate the roughness of the surface of PEDOT/ZnO/PMMA sheets, Figure 4.6 shows high-resolution tapping-mode AFM images of PEDOT/ZnO/PMMA sheet compared with one without the ZnO layer. Figure 4.6a indicated that the PEDOT/PMMA sheets had high number of dark area indicating the flat surface with the small roughness (23 nm) as shown in Table 4.4. The smooth surface of the PEDOT/PMMA sheet was also observed in the SEM image. When the ZnO layer was inserted between PEDOT and PMMA by using 10 wt% ZnO in the PMMA syrup, the roughness of the modified PMMA sheet was increased to 46 nm (Figure 4.6b). However, the use of ZnO concentration in the PMMA syrup at 34 and 58 wt% decreased the roughness of the

modified PMMA sheet to 30–32 nm as shown in Figure 4.6c and 4.6d. This was possibly due to the greater ZnO grain size obtained from the higher ZnO content in the PMMA syrup as also observed in the SEM images.

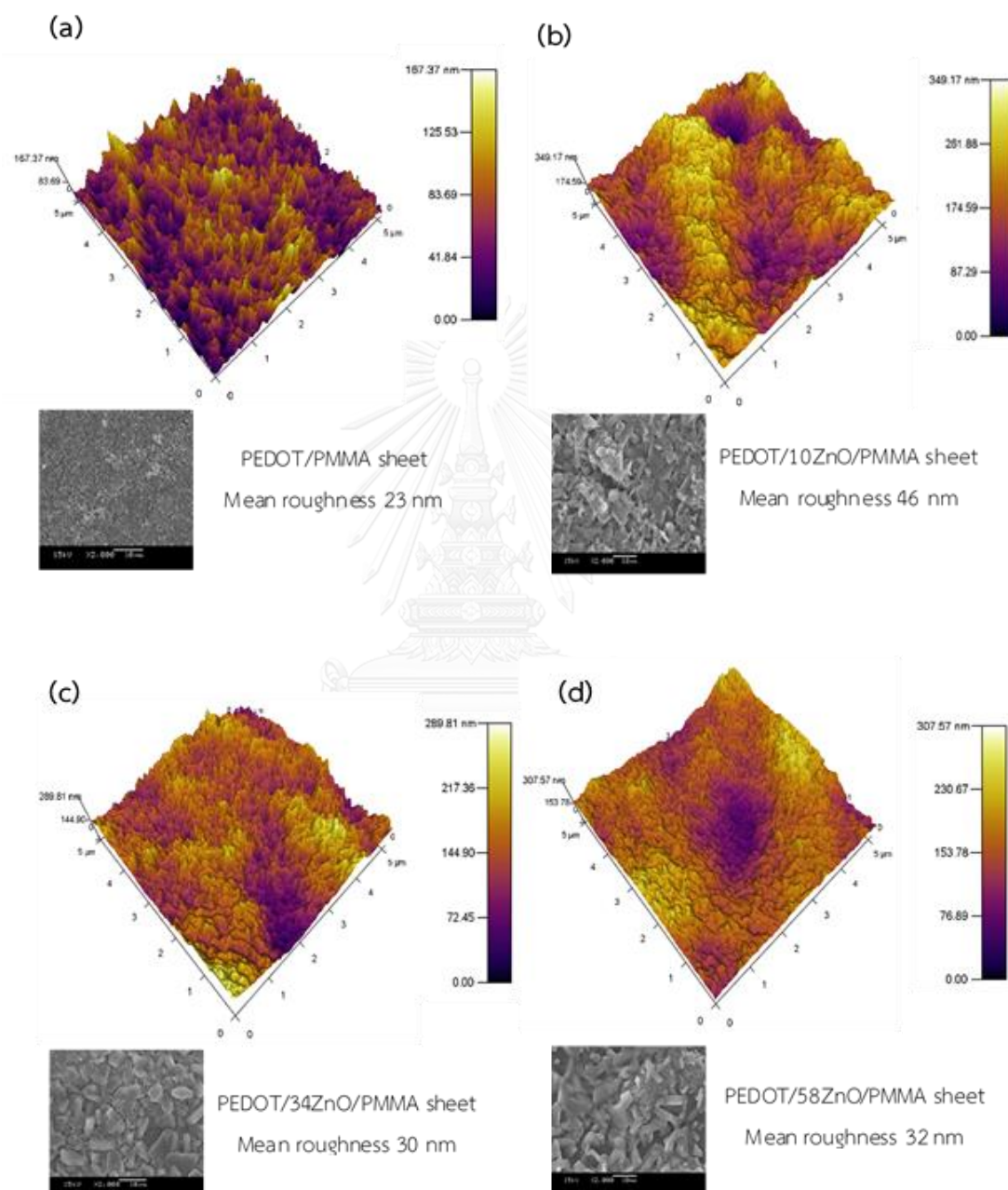


Figure 4.6 AFM and SEM images of (a) PEDOT/PMMA sheets and PEDOT/ZnO/PMMA sheets obtained from (b) 10 wt% (c) 34 wt% and (d) 58 wt% ZnO concentration in the PMMA syrup.

To consider the electrical resistance of the modified PMMA sheets, the result in Table 4.4 showed that the electrical resistance of the modified PMMA sheets tended to be increased with increasing the ZnO concentration in the PMMA syrup due to the effect of ZnO having poor electrical conductivity (Wang, Wei, and Hu 2013).

Table 4.4 The effect of ZnO concentration in the PMMA syrup on the roughness and electrical resistance of the modified PMMA sheets.

ZnO concentration in the PMMA syrup (wt%)	rms roughness (nm)	Electrical resistance (Ω/cm^2)
0	23	30.7 ± 1.39
10	46	31.4 ± 2.52
34	30	33.2 ± 2.09
58	32	34.2 ± 5.23

4.5 Electrochemical properties of modified PMMA counter electrode measured by cyclic voltammetry (CV)

Counter electrode plays a major role in collecting high energy electrons from external circuit and oxidizing I_3^- species in electrolyte back to I^- state at the electrolyte/counter electrode interface. To further investigate the electrocatalytic activity of the counter electrode, the cyclic voltammogram was studied. The redox activity of the Pt, bare FTO, PEDOT and PEDOT/ZnO films in an electrolyte was demonstrated in Figure 4.7. A broad potential window scan was initially carried out for Pt-based counter electrode to identify the possible redox reaction of the system as seen in Figure 4.7a. Four redox peaks were observed as followed: peaks no. 1 and no. 2 were assigned to cathodic and anodic peaks of the I_3^-/I^- couple, respectively, whereas peak no. 3 and no. 4 were those of the I_3^-/I_2 couple (Biallozor and Kupniewska 2000). The reaction rate of I_3^- ion in the electrolyte was characterized by the cathodic peak

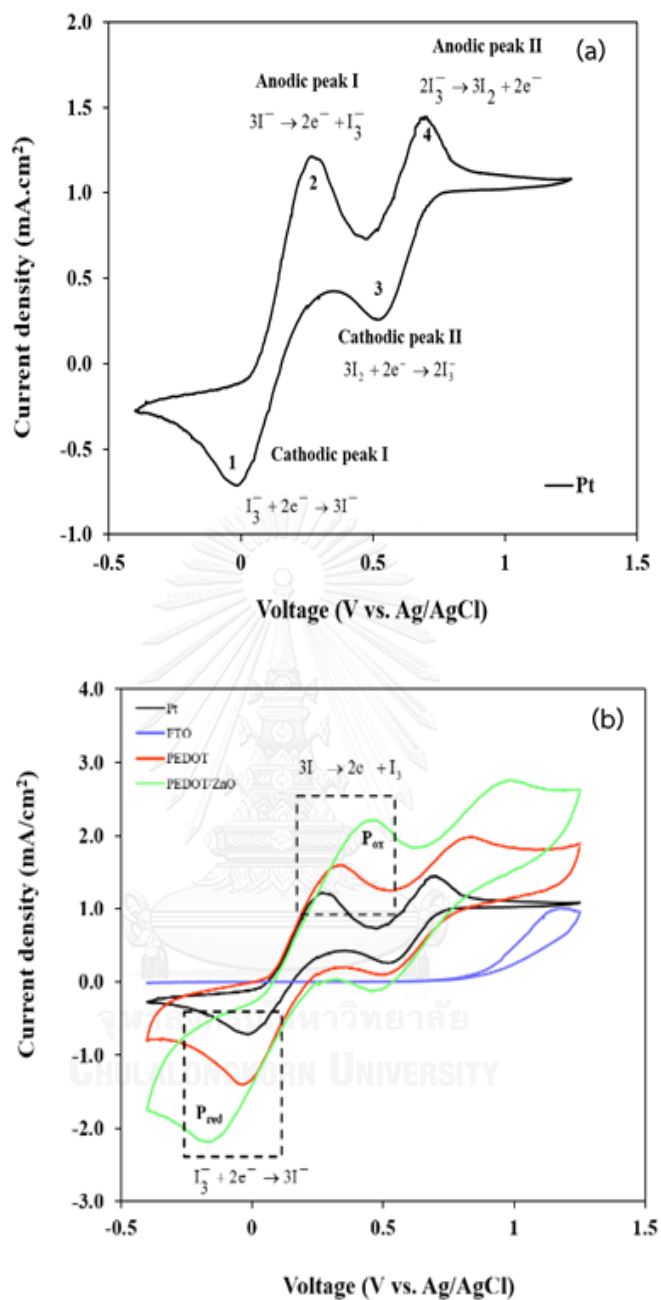


Figure 4.7 Cyclic voltammograms of (a) Pt counter electrode and (b) PEDOT/ZnO/FTO (prepared from 10 wt% ZnO in PMMA syrup) compared to FTO with and without Pt at a scan rate of 20 mV/s in 0.01M LiI and 0.001M I₂ in acetonitrile solution containing 0.1M LiClO₄ used as the supporting electrolyte.

current density (I_{CP}) in the CV curve. Higher I_{CP} absolute value implied a better electrocatalytic activity of the catalytic material (Hauch and Georg 2001). To compare the catalytic activity of electrodes, a convenient parameter called the peak-to-peak separation, E_{pp} , defined as $|E_{AP} - E_{CP}|$ is often measured where E_{AP} and E_{CP} are the anodic and cathodic potentials, respectively.

In Figure 4.7b the cyclic voltammograms of I_3^-/I^- redox electrolyte on Pt, bare FTO, PEDOT and PEDOT/ZnO counter electrodes were presented. Two typical I_3^-/I^- redox reaction peaks were observed as Pt, PEDOT or PEDOT/ZnO were used as working electrode in the experimental setup. The bare FTO showed poor catalytic behaviour without oxidation/reduction peaks. Both PEDOT films showed comparable catalytic behaviour relative to that of Pt electrode, suggesting that PEDOT could also promote the electron transport between the redox mediator and counter electrodes (Wei et al. 2007). In addition, the PEDOT-ZnO counter electrode generated I_{CP} of 2.25 mA/cm^2 , higher than that of Pt (0.75 mA/cm^2) and PEDOT (1.40 mA/cm^2) counter electrodes suggesting a faster rate of redox reaction, higher electrical conductivity and higher cathodic current density of the PEDOT-ZnO material over the others. This result promoted that the PEDOT/ZnO was the most probable material among all for DSSC counter electrode application. Detailed CV results were summarized in Table 4.5.

Simultaneously, the diffusion coefficient (D_n) is proportional to the I_{CP} which obeys the Randles-Sevcik equation as shown in Eq. 4.2.

$$I_{CP} = Kn^{1.5} AC(D_n)^{0.5} \nu^{0.5} \quad (4.2)$$

where I_{CP} is the cathodic current densities; K is a constant having a value of 2.69×10^5 ; n is the number of electrode contributing to the charge transfer (here, $n = 2$); A is the area of the counter electrode; C and ν represent the concentration of I_3^- species and the scan rate, respectively. The diffusivity for the PEDOT/ZnO counter electrode is

Table 4.5 Electrochemical characteristics of Pt, bare FTO, PEDOT and PEDOT/ZnO electrodes

Counter electrode	I_{CP} (mA)	I_{AP} (mA)	E_{CP} (V)	E_{AP} (V)	E_{PP} (V)
Pt	-0.75	1.25	0.02	0.27	0.25
PEDOT	-1.40	1.60	0.03	0.30	0.27
PEDOT-ZnO	-2.25	2.28	-0.18	0.45	0.63

slightly larger than that of Pt and PEDOT counter electrodes, presumably due to the higher surface roughness of the counter electrode (Yue et al. 2014).

4.6 Performance of DSSC based on FTO and different counter electrodes

The photovoltaic tests of the DSSC with an exposed area of 0.25 cm² were carried out by measuring photocurrent-voltage (*I-V*) characteristic curves under standard light irradiation of 100 mW/cm² (AM 1.5 G) from solar simulator in an ambient atmosphere. The fill factor (FF) and the overall photo conversion efficiency (PCE, η) of the solar cell were calculated according to the following equations (Xiao et al. 2012).

$$\eta = \frac{P_{\max}}{P_{\text{light}}} \times 100\% = \frac{V_{oc} \times J_{sc} \times FF}{P_{\text{light}}} \times 100\% \quad (4.3)$$

$$FF = \frac{P_{\max}}{V_{oc} \times I_{sc}} = \frac{(V \times J)_{\max}}{V_{oc} \times J_{sc}} \quad (4.4)$$

where J_{sc} is the short-circuit current density (mA/cm²), V_{oc} is the open-circuit voltage (V), P_{light} is the incident light power, J_{\max} (mA/cm²) and V_{\max} (V) are the current density and voltage at the point of maximum power output in the *I-V* curve, respectively.

Figure 4.8 presents the *I-V* characteristic of DSSC with counter electrodes made from Pt, FTO, PEDOT/FTO, PEDOT/glass, PEDOT/PMMA, and PEDOT/ZnO/PMMA and

Table 4.6 summarizes the performance data of all cells. It was observed that the conventional DSSC using Pt and FTO-conductive glass (Entry 1) exhibited the high V_{OC} , J_{SC} and FF values with low $R_{(series)}$ resulting in the high energy conversion efficiency ($\eta = 3.6\%$). Although Pt plays an important role to collect electrons and catalyze I_3^-/I^- redox- reaction for DSSC, it is very expensive and requires high temperature for thermal reduction of Pt^{4+} to Pt^0 to be used for catalyzing the redox reaction of iodide electrolyte (Feltham and Spiro 1971).

As clearly shown in Table 4.6, PEDOT electrode could simultaneously perform both catalytic activity and electrical conductivity in the DSSC. When the PEDOT layer deposited on an inert glass was used as the counter electrode, it decreased the DSSC's series resistance down by 94% compared to the cell based on commercial FTO glass (Entry 2 vs.Entry 4). In addition, no significant difference in cell's series resistance has been made by FTO glass counter electrodes covered with either Pt or PEDOT (Entry 1 vs. Entry 3). DSSC with pure FTO glass counter electrode (Entry 2) delivered poor efficiency due to slow oxidation reaction of I_3^- species. Owing to PEDOT layer,

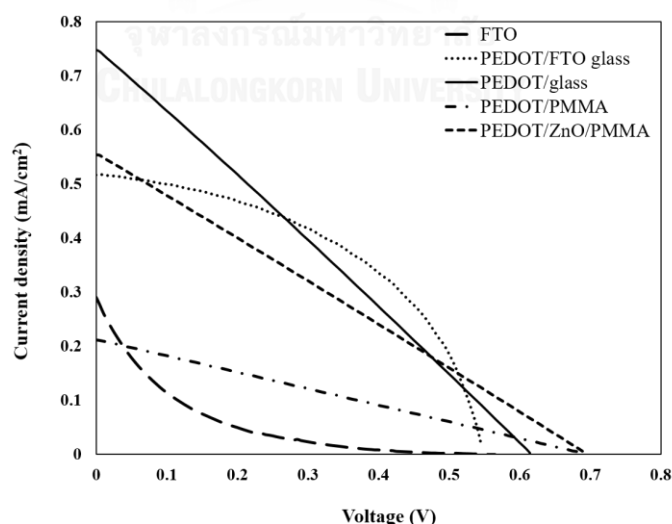


Figure 4.8 Comparative I-V curves of DSSC with different counter electrodes made from FTO glass, PEDOT/glass, PEDOT/PMMA, and PEDOT/ZnO/PMMA (10 wt% ZnO in the PMMA syrup).

Table 4.6 Photovoltaic performance of DSSC using various kinds of counter electrode

Entry	Counter electrode	V_{oc} (mV)	J_{sc} (mA/cm ²)	FF	$R_{(series)}$ (Ω/cm^2)	η (%)
1	Pt/FTO glass	740	7.08	0.70	11.1	3.60
2	FTO glass	570	0.29	0.07	12,930	0.01
3	PEDOT/FTO glass	550	0.51	0.48	11.2	0.14
4	PEDOT/glass	615	0.75	0.26	770	0.12
5	PEDOT/PMMA sheet	695	0.21	0.25	3,219	0.04
6	PEDOT/ZnO/PMMA sheet	695	0.55	0.26	1,206	0.10
7	PEDOT/ZnO/PMMA sheet	321	0.08	0.26	3,635	0.01
8	PEDOT/ZnO/PMMA sheet	585	0.04	0.23	13,110	0.005
9	2-methylimidazole/ PEDOT/ZnO/PMMA sheet	670	0.09	0.27	6,548	0.02

*Condition: Dye Z907, surlyn 60 μ m, TiO₂ 3 layers (thickness 9 μ m), temperature 120 °C, pressure 2 MP, liquid electrolyte (HI-30).

**Entry 6, 7 and 8 prepared from 10 wt%, 34 wt% and 58 wt% ZnO in the PMMA syrup, respectively.




***Entry 9 prepared from 10 wt% ZnO in the PMMA syrup, respectively.

he current density and the fill factor were improved and the cell yielded 0.14% η (Entry 3). This reflected the catalytic activity of PEDOT in DSSC (Yohannes and Inganäs 1998). The photocurrent and photovoltage of DSSC made by PEDOT/inert glass (Entry 4) appeared higher than those of DSSCs made by PEDOT/FTO glass (Entry 3) at open-circuit and short-circuit conditions, suggesting the more-negative energy level shift of FTO material with reference to the plain glass. However, when the glass substrate was replaced by PMMA sheet, the cell's performance was significantly dropped. This might

be resulted from an inequality in sheet resistance between anode and cathode substrate (FTO glass for anode vs. PMMA sheet for cathode) causing non-homogeneous current density over the cell area. To improve the cell performance, a thin layer of ZnO material has been introduced in between PEDOT layer and the PMMA substrate. In contrast to PEDOT, ZnO strongly interacts with I_3^- species in electrolyte; thus, the PEDOT/ZnO combination enhanced the catalytic activity of DSSC counter electrode compared to one using PEDOT alone (Wang, Wei, and Hu 2013). The DSSC test results denote twofold rising of current density and η values in case of PEDOT/ZnO/PMMA substrate prepared by 10 wt% ZnO in the PMMA syrup (Entry 6). The performance of DSSCs employing PEDOT/ZnO/PMMA substrates prepared by 34 wt% and 58 wt% ZnO in the PMMA syrup were also evaluated as shown in Entry 7 and Entry 8, respectively. Obviously, high ZnO contents increased the cell's series resistance resulting in the reduction of current density. The result agrees well with the sheet surface resistance discussed in Section 4.4.3.

Although the section 4.3 showed that the addition of 2-methylimidazole (3-5 M) could decrease the electrical resistance of PEDOT/PMMA sheets from $30.65 \Omega/\text{cm}^2$, the DSSC consisted of 2-methylimidazole/PEDOT/ZnO/PMMA sheet as the counter electrode provided only 0.02% η . This could be explained by using the surface property measured by microscope equipped to determine the water contact angle of surface of each electrode as seen in Table 4.7. It was observed that the surface of 2-methylimidazole/PEDOT/ZnO/PMMA sheet exhibited low water contact angle as 37.15° reflecting the high hydrophilicity, while the surface of surlyn used as the binder of two electrodes of DSSC exhibited the high water contact angle as 98.40° . This indicated that surlyn surface had lower polarity, which might not be well adhered to the surface of 2-methylimidazole/PEDOT/ZnO/PMMA sheet resulting in the leakage of electrolyte. To consider the PEDOT/ZnO/PMMA sheet, its surface showed the water contact angle as 82.85° , which was similar to surlyn.

Table 4.7 The contact angle of water on the surface of surlyn, PEDOT/ZnO/PMMA sheet, 2-methylimidazole/PEDOT/ZnO/PMMA sheet

Sample	Appearance	Water contact angle (°)
surlyn		98.40 ± 1.35
2-methylimidazole/ PEDOT/ZnO/PMMA sheet		37.15 ± 2.31
PEDOT/ZnO/PMMA sheet		82.85 ± 2.49

This implied that PEDOT/ZnO/PMMA sheet had similar degree of polarity to surlyn providing good adhesion with on leakage of electrolyte resulting in the better DSSC performance.

4.7 Incident photo-to-current efficiency (IPCE)

To determine the spectral response of DSSC device based on PEDOT/ZnO/PMMA, the incident photon-to-current conversion efficiency (IPCE) spectrum was measured. IPCE is defined as a ratio of photo current (I_{ph}) to the power input (P_{in}) as shown in Eq. 4.5

$$IPCE(\lambda) = I_{ph} / (q\lambda / hc * P_{in}) \quad (4.5)$$

where q is an elementary charge, h is Planck's constant (6.63×10^{-34} J.s) and c is the speed of light (3×10^8 m/s).

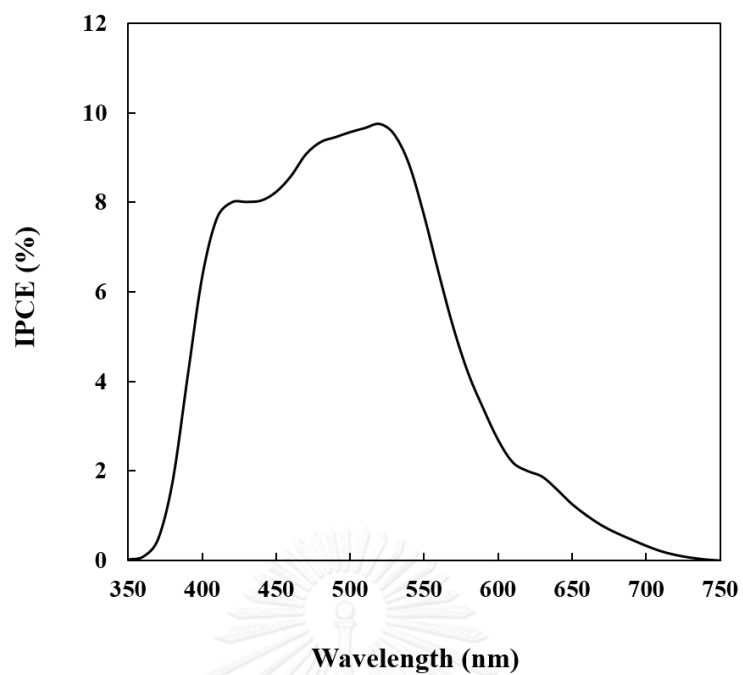


Figure 4.9 IPCE of DSSC with modified PMMA sheet as counter electrode.

The IPCE result showed a broad spectrum in range between 350 – 750 nm as illustrated in Figure 4.9, suggesting that the DSSC device based on PEDOT/ZnO/PMMA could efficiently convert incident photons into electricity in this region. A peak value of 9.8% was observed at 520 nm, corresponding to the second Q-band of the absorption spectrum of the Z907 dye in the solution (Polizotti et al. 2012).

CHAPTER V

CONCLUSION

5.1 Conclusion

5.1.1 Enhancement of electrical conductivity of poly(methyl methacrylate) (PMMA) sheet via spin coating of 3,4-ethylenedioxythiophene (EDOT) monomer

The electrical resistance of PMMA sheets could be decreased via *in situ* polymerization of EDOT using spin coating technique. The solution of PEDOT containing Fe (III) p-toluene sulfonate and pyridine to produce poly(3,4-ethylenedioxythiophene) (PEDOT) onto PMMA sheets. The result indicated that the spinning rate of 300 rpm for 30 s induced the PMMA surface with the minimum electrical resistance as $30.65 \Omega/\text{cm}^2$. To enhance the conductivity of PEDOT, the addition of organic compound as 2-methylimidazole, which can rearrange the PEDOT segment led the better connections between the conducting PEDOT chains. The reduction of electrical resistance of PEDOT/PMMA sheet was also depended on the concentration of 2-methylimidazole. The increase in the concentration of 2-methylimidazole to 5 M could decrease the electrical resistance of PEDOT/PMMA sheet from $30.65 \Omega/\text{cm}^2$ to $12 \Omega/\text{cm}^2$, which was lower than that of FTO glass ($20 \Omega/\text{cm}^2$).

5.1.2 Effect of zinc oxide layer on the properties of modified PMMA sheets (PEDOT/ZnO/PMMA sheets)

PEDOT had potential for catalyzing the redox reaction of electrolyte for dye-sensitized solar cell (DSSC). The incorporation of PEDOT with zinc oxide (ZnO) increased the energy conversion efficiency of electrical device such as DSSC depended

on the amount of ZnO. ZnO can strongly absorb I_3^- . In contrast, I_3^- has weaker interaction with PEDOT. Therefore, ZnO would have a higher catalytic activity than PEDOT for I_3^- reduction. Thus, this research attempted to insert ZnO layer between PEDOT and PMMA by using 10 wt% ZnO in the PMMA syrup via spin coating technique at 3,000 rpm for 30 s. The roughness of the modified PMMA sheets with ZnO layer was increased from 23 nm to 46 nm. Determined by atomic force microscopy (AFM). This implies that the charge-transfer resistance at counter electrode/electrolyte interface would be lower to give more reaction site for reducing I_3^- to form I^- in the electrolyte.

5.1.3 Performance of DSSC

From the cyclic voltammograms (CVs) measurement, it was observed that PEDOT had the potential to be the catalyst for redox reaction of I_3^-/I^- . When the ZnO layer was inserted between PEDOT and PMMA sheet, the surface of PEDOT/ZnO/PMMA sheet had higher roughness reflecting the higher catalytic area to provide the better energy conversion efficiency (η). It was observed that DSSC consisted of PEDOT/ZnO/PMMA sheet used as the counter electrode provided 150% higher η than DSSC based on PEDOT/PMMA counter electrode.

5.2 Recommendations

1. Although PEDOT had potential for using as the catalyst for I_3^-/I^- redox reaction, it still showed lower efficiency than Pt catalyst. Thus, the preparation of Pt on the surface of polymeric substrates at low temperature should be investigated.
2. For the photoanode, the synthesis of anatase-TiO₂ at low temperature should be further explored for the DSSC consisted of polymeric electrodes.
3. Since the normal electrolyte used in DSSC is dissolved in acetonitrile, which can damage the PMMA substrate, the investigation of suitable solvent for

electrolyte used in the DSSC made from the PMMA-base electrode should be suggested.

4. For the counter electrode, the preparation of ZnO solution in PMMA syrup less than 10 wt% should be recommended to improve energy conversion efficiency for DSSC performance.



REFERENCES

- Abdiryim, T., Ali, A., Jamal, R., Osman, Y., and Zhang, Y. 2014. 'A facile solid-state heating method for preparation of poly(3,4-ethylenedioxythiophene)/ZnO nanocomposite and photocatalytic activity', *Nanoscale Research Letter*, 9: 1-8.
- Asbury, J. B., Hao, E., Wang, Y., Ghosh, H. N., and Lian, T. 2001. 'Ultrafast electron transfer dynamics from molecular adsorbates to semiconductor nanocrystalline thin films', *Physical Chemistry*, 105: 4545-57.
- Benko, G., Kallioinen, J., Korppi-Tommola, J. E. I., Yartsev, A. P., and Sundstrom, V. 2002. 'Photoinduced ultrafast dye-to-semiconductor electron injection from nonthermalized and thermalized donor states', *American Chemical Society*, 124: 489-93.
- Bialozor, S., and Kupniewska, A. 2000. 'Study on poly(3,4-ethylenedioxythiophene) behaviour in I⁻/I₂ solution', *Electrochemistry Communications*, 2: 480-86.
- Chen, J. G., Wei, H. Y., and Ho, K. C. 2007. 'Using modified poly(3,4-ethylene dioxythiophene): poly(styrene sulfonate) film as a counter electrode in dye-sensitized solar cells', *Solar Energy Materials and Solar Cells*, 91: 1472-77.
- Chen, L., Tan, W., Zhang, J., Zhou, X., Zhang, X., and Lin, Y. 2010. 'Fabrication of high performance Pt counter electrodes on conductive plastic substrate for flexible dye-sensitized solar cells', *Electrochimica Acta*, 55: 3721-26.
- Elschner, A., Kirchmeyer, S., Lovenich, W., Merker, U., and Reuter, K. 2011. *PEDOT principle and applications of an intrinsically conductive polymer* (CRC Press Taylor and Francis Group, LLC: New York).
- Feltham, A. M., and Spiro, M. 1971. 'Platinized platinum electrodes', *Chemical Reviews*, 71: 177-93.
- Fine, G. F., Cavanagh, L. M., Afonja, A., and Binions, R. 2010. 'Metal oxide semi-conductor gas sensors in environmental monitoring', *Sensors (Basel)*, 10: 5469-502.

- Fortunato, E., Barquinha, P., Pimentel, A., Gonçalves, A., Marques, A., Pereira, L., and Martins, R. 2005. 'Recent advances in ZnO transparent thin film transistors', *Thin Solid Films*, 487: 205-11.
- Garganourakis, M., Logothetidis, S., Pitsalidis, C., Georgiou, D., Kassavetis, S., and Laskarakis, A. 2009. 'Deposition and characterization of PEDOT/ZnO layers onto PET substrates', *Thin Solid Films*, 517: 6409-13.
- Goseki, R., and Ishizone, F. 2015. 'Encyclopedia of polymeric nanomaterials: poly(methyl methacrylate)', *Springer-Verlag Berlin Heidelberg*: 1702-10.
- Grätzel, M. 2001. 'Photochemical cells', *Macmillan Magazines Ltd*, 414: 338-44.
- Grätzel, M. 2003. 'Dye-sensitized solar cells', *Journal of Photochemistry and Photobiology C: Photochemistry Reviews*, 4: 145-53.
- Groenrndaal, L. B., Gianni, Z., Aubert, P. H., Waybright, S. M., and Reynolds, J. R. 2003. 'Electrochemistry of poly(3,4-alkylenedioxythiophene) derivatives', *Advance materials*, 15: 855-79.
- Groenrndaal, L. B., Jonas, F., Freitag, D., Pielartzik, H., and Reynolds, J. R. 2000. 'Poly(3,4-etylenedioxythiophene) and its derivatives: past, present, and future', *Advance materials*, 12: 481-94.
- Hagfeldt, A., and Grätzel, M. 1995. 'Light induced redox reactions in nanocrystalline systems', *American Chemical Society*, 95: 49-68.
- Hansen, T. S., West, K., Hassager, O., and Larsen, N. B. 2006. 'Integration of conducting polymer network in non-conductive polymer substrates', *Synthetic Metals*, 156: 1203-07.
- Haque, S. A., Palomares, E., Cho, B. M., Green, A. N. M., Hirata, N., Klug, D. R., and Durrant, J. R. 2005. 'Charge separation versus recombination in dye-sensitized: the minimization of kinetic redundancy', *American Chemical Society*, 127: 3456-62.
- Hauch, A., and Georg, A. 2001. 'Diffusion in the electrolyte and charge-transfer reaction at the platinum electrode in dye-sensitized solar cells', *Electrochimica Acta*, 46: 3457-66.

- Imoto, K., Takahashi, K., Yamaguchi, T., Komura, T., Nakamura, J. I., and Murata, K. 2003. 'High-performance carbon counter electrode for dye-sensitized solar cells', *Solar Energy Materials and Solar Cells*, 79: 459-69.
- Kavan, L., Liska, P., Zakeeruddin, S. M., and Grätzel, M. 2016. 'Low-temperature fabrication of highly-efficient, optically-transparent (FTO-free) graphene cathode for Co-mediated dye-sensitized solar cells with acetonitrile-free electrolyte solution', *Electrochimica Acta*, 195: 34-42.
- Kelly, C. A., Farzad, F., Thompson, D. W., Stipkala, J. M., and Meyer, G. J. 1999. 'Cation-controlled interfacial charge injection in sensitized nanocrystalline TiO₂', *Langmuir*, 15: 7047-54.
- Kim, J. W., Kim, N. H., Kuilla, T., Kim, T. J., Rhee, K. Y. and Lee, J. H. 2010. 'Synergy effects of hybrid carbon system on properties of composite bipolar plates for fuel cells', *Journal of Power Sources*, 195: 5474-80.
- Kim, M. R., Park, S. H., Kim, J. U., and Lee, J. K. 2011. 'Dye-sensitized solar cells based on polymer electrolytes, solar cells-dye-sensitized devices.' in 10 (ed.).
- Kim, S. S., Nah, Y. C., Noh, Y. Y., Jo, J., and Kim, D. Y. 2006. 'Electrodeposited Pt for cost-efficient and flexible dye-sensitized solar cells', *Electrochimica Acta*, 51: 3814-19.
- Kirchmeyer, S., and Reuter, K. 2005. 'Scientific importance, properties and growing applications of poly(3,4-ethylenedioxythiophene)', *Journal of Materials Chemistry*, 15: 2077-88.
- Kraft, A., Grimsdale, A. C., and Holmes, A. B. 1998. 'Electroluminescent conjugated polymers-seeing polymers in a new light', *Angewandte Chemie International Edition*, 37: 402-28.
- Krebs, F. C. 2009. 'Fabrication and processing of polymer solar cells: A review of printing and coating techniques', *Solar Energy Materials and Solar Cells*, 93: 394-412.
- Kulyk, B., Kapustianyk, V., Tsybulskyy, V., Krupka, O., and Sahraoui, B. 2010. 'Optical properties of ZnO/PMMA nanocomposite films', *Journal of Alloys and Compounds*, 502: 24-27.

- Lenzmann, F. O., and Kroon, J. M. 2007. 'Recent Advances in dye-sensitized solar cells', *Advances in OptoElectronics*, 2007: 1-10.
- Li, B., Wang, L., Kang, B., Wang, P., and Qiu, Y. 2006. 'Review of recent progress in solid-state dye-sensitized solar cells', *Solar Energy Materials and Solar Cells*, 90: 549-73.
- Lu, G., Qu, L., and Shi, G. 2005. 'Electrochemical fabrication of neuron-type networks based on crystalline oligopyrene nanosheets', *Electrochimica Acta*, 51: 340-46.
- Markvart, T., and Castañer, L. 2013. 'Principles of solar cell operation': 3-25.
- Mastragostino, M., Arbizzani, C., and Soavi, F. 2002. 'Conducting polymers as electrode materials in supercapacitors', *Solid State Ionics*, 148: 493-98.
- Mens, R., Adriaensens, P., Lutsen, L., Swinnen, A., Bertho, S., Ruttens, B., D'Haen, J., Manca, J., Cleij, T., Vanderzande, D., and Gelan, J. 2008. 'NMR study of the nanomorphology in thin films of polymer blends used in organic PV devices: MDMO-PPV/PCBM', *Journal of Polymer Science Part A: Polymer Chemistry*, 46: 138-45.
- Murakami, T. N., and Grätzel, M. 2008. 'Counter electrodes for DSC', *Inorganica Chimica Acta*, 361: 572-80.
- Nogueira, A. F., Longo, C., and De Paoli, M. A. 2004. 'Polymers in dye sensitized solar cells: overview and perspectives', *Coordination Chemistry Reviews*, 248: 1455-68.
- O'Regan, B., and Grätzel, M. 1991. 'A low-cost, high-efficiency solar cell based on dye-sensitized colloidal TiO₂ films', *Nature Publishing Group*, 353: 737-39.
- Oskam, G., Bergerom, B. V., Meyer, G. J., and Searson, P. C. 2001. 'Pseudohalogens for dye-sensitized TiO₂ photoelectrochemical cell', *Physical Chemistry*, 105: 6867-73.
- Pimentel, A., Fortunato, E., Gonçalves, A., Marques, A., Águas, H., Pereira, L., Ferreira, I., and Martins, R. 2005. 'Polycrystalline intrinsic zinc oxide to be used in transparent electronic devices', *Thin Solid Films*, 487: 212-15.

- Polizotti, A., Schual-Berke, J., Falsgraf, E., and Johal, M. 2012. 'Investigate new materials and architectures for Grätzel cells.' in V. Fthenakis (ed.), *Third generation photovoltaics* (InTech).
- Quintana, M., Edvinsson, T., Hagfeldt, A., and Boschloo, G. 2007. 'Comparison of dye-sensitized ZnO and TiO₂ solar cells studies of charge transport and carrier lifetime', *Phys Chem*, 111: 1035-41.
- Saghaei, J., Fallahzadeh, A., and Yousefi, M. H. 2015. 'Improvement of electrical conductivity of PEDOT:PSS films by 2-Methylimidazole post treatment', *Organic Electronics*, 19: 70-75.
- Sahito, I. A., Sun, K. C., Arbab, A. A., Qadir, M. B., Choi, Y. S., and Jeong, S. H. 2016. 'Flexible and conductive cotton fabric counter electrode coated with graphene nanosheets for high efficiency dye sensitized solar cell', *Journal of Power Sources*, 319: 90-98.
- Saito, Y., Kubo, W., Kitamura, T., Wada, Y., and Yanagida, S. 2004. 'I⁻/I₃⁻ redox reaction behavior on poly(3,4-ethylenedioxythiophene) counter electrode in dye-sensitized solar cells', *Journal of Photochemistry and Photobiology A: Chemistry*, 164: 153-57.
- Sakurai, S., Jiang, H. Q., Takahashi, M., and Kobayashi, K. 2009. 'Enhanced performance of a dye-sensitized solar cell with a modified poly(3,4-ethylenedioxythiophene)/TiO₂/FTO counter electrode', *Electrochimica Acta*, 54: 5463-69.
- Saranya, K., Rameez, M., and Subramania, A. 2015. 'Developments in conducting polymer based counter electrodes for dye-sensitized solar cells – An overview', *European Polymer Journal*, 66: 207-27.
- Schilinsky, P., Waldauf, C., and Brabec, C. J. 2006. 'Performance analysis of printed bulk heterojunction solar cells', *Advanced Functional Materials*, 16: 1669-72.
- Stier, W., Duncan, W. R., and Prezhdo, O. V. 2004. 'Thermally assisted sub-10 fs electron transfer in dye-sensitized nanocrystalline TiO₂ solar cells', *Advanced Materials*, 16: 240-44.

- Subramanian, M. N. 2014. 'Introduction to polymer compounding raw materials', *Smithers Papra Technology Ltd.*, 1: 14-15.
- Susmitha, K., Kumar, M. N., Rajkumar, G., Giribabu, L., and Raghavender, M. 2015. 'Enhanced dye sensitized solar cell performance with high surface area thin ZnO film and PEDOT:PSS', *Solar Energy*, 118: 126-33.
- Wang, H., Wei, W., and Hu, Y. H. 2013. 'Efficient ZnO-based counter electrodes for dye-sensitized solar cells', *Journal of Materials Chemistry A*, 1: 6622.
- Wei, D. 2010. 'Dye sensitized solar cells', *Int J Mol Sci*, 11: 1103-13.
- Wei, T. C., Wan, C. C., Wang, Y. Y., Chen, C. M., and Shiu, H. S. 2007. 'Immobilization of poly(N-vinyl-2-pyrrolidone)-capped platinum nanoclusters on indium-tin oxide glass and its application in dye-sensitized solar cells', *Phys Chem*, 111: 4847-53.
- Woodley, S. M., and Catlow, C. R. A. 2009. 'Structure prediction of titania phases: implementation of Darwinian versus Lamarckian concepts in an evolutionary algorithm', *Computational Materials Science*, 45: 84-95.
- Wu, C., Chen, B., Zheng, X., and Priya, S. 2016. 'Scaling of the flexible dye sensitized solar cell module', *Solar Energy Materials and Solar Cells*, 157: 438-46.
- Wu, J., Li, Q., Fan, L., Lan, Z., Li, P., Lin, J., and Hao, S. 2008. 'High-performance polypyrrole nanoparticles counter electrode for dye-sensitized solar cells', *Journal of Power Sources*, 181: 172-76.
- Xia, J., Masaki, N., Jiang, K., and Yanagida, S. 2007. 'The influence of doping ions on poly(3,4-ethylenedioxythiophene) as a counter electrode of a dye-sensitized solar cell', *Journal of Materials Chemistry*, 17: 2845.
- Xiao, Y. M., Lin, J. Y., Wu, J. H., Tai, S. Y., and Yue, G. T. 2012. 'Pulse potentiostatic electropolymerization of high performance PEDOT counter electrodes for Pt-free dye-sensitized solar cells', *Electrochimica Acta*, 83: 221-26.
- Yohannes, T., and Inganäs, O. 1998. 'Photoelectrochemical studies of the junction between poly[3-(4-octylphenyl)thiophene] and a redox polymer electrolyte', *Solar Energy Materials and Solar Cells*, 51: 193-202.

- Yue, G., Li, F., Tan, F., Li, G., Chen, C., and Wu, J. 2014. 'Nickel sulfide films with significantly enhanced electrochemical performance induced by self-assembly of 4-aminothiophenol and their application in dye-sensitized solar cells', *RSC Adv.*, 4: 64068-74.
- Yun, H. G., Kim, M., Kang, M. G., and Lee, I. H.. 2012. 'Cost-effective dye-sensitized solar cells consisting of two metal foils instead of transparent conductive oxide glass', *Physical Chemistry Chemical Physics*, 14: 6448-51.
- Zhang, L., Li, F., Chen, Y., and Wang, X. 2011. 'Synthesis of transparent ZnO/PMMA nanocomposite films through free-radical copolymerization of asymmetric zinc methacrylate acetate and in-situ thermal decomposition', *Journal of Luminescence*, 131: 1701-06.
- Zhang, Y., Zhuang, S., Xu, X., and Hu, J. 2013. 'Transparent and UV-shielding ZnO@PMMA nanocomposite films', *Optical Materials*, 36: 169-72.
- Zhou, H., Shi, Y., Qin, D., An, J., Chu, L., Wang, C., Wang, Y., Guo, W., Wang, L., and Ma, T. 2013. 'Printable fabrication of Pt-and-ITO free counter electrodes for completely flexible quasi-solid dye-sensitized solar cells', *Journal of Materials Chemistry A*, 1: 3932.



APPENDIX

จุฬาลงกรณ์มหาวิทยาลัย
CHULALONGKORN UNIVERSITY

APPENDIX A

Example of conductivity calculation of the modified PMMA sheets

The electrical conductivity (σ (S/cm)) of the surface of each specimens is calculated from Eq.1 and 2 as shown below:

$$\rho = R_s \times t \quad (1)$$

$$\sigma = \frac{1}{\rho} \quad (2)$$

where t = sample thickness (cm) of the PEDOT layer on PMMA sheets

R_s = the sheet resistance (Ω/cm^2) of the specimens

ρ = the electrical resistivity ($\Omega\cdot\text{cm}$).

From the spin coating PEDOT onto PMMA sheets, all obtained data for modified PMMA sheet (condition: 0.22 mL EDOT monomer at 300 rpm spinning rate for 30 s spinning time) was calculated as shown below:

Thickness (t)	= 0.00023 cm
Sheet resistance (R_s)	= 30.65 Ω/cm^2
Electrical resistivity (ρ)	= $t \times R_s$
	= 0.00023 \times 30.65
	= 0.007 $\Omega\cdot\text{cm}$
Electrical conductivity (σ)	= $\frac{1}{\rho} = \frac{1}{0.007} = 142.7$ S/cm

APPENDIX B

Comparison of thickness between FTO glass and PEDOT film on PMMA sheets

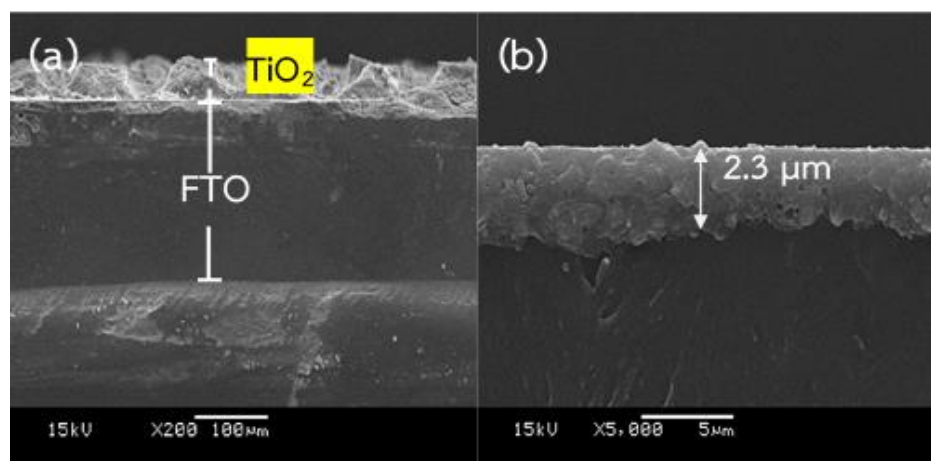


Figure B1. SEM images of the cross-section of FTO glass compare to the modified PMMA sheets having PEDOT film obtained from the spinning rate of 300 rpm.

APPENDIX C

The thickness images of TiO₂ film on FTO glass

The thickness of TiO₂ film was examined using surface profilometer (3ST, Dektak, USA). A screen with 90T mesh was used to obtain ~ 3 μm TiO₂ film thickness for 1 layer and ~ 9 μm TiO₂ film thickness for 3 layers.

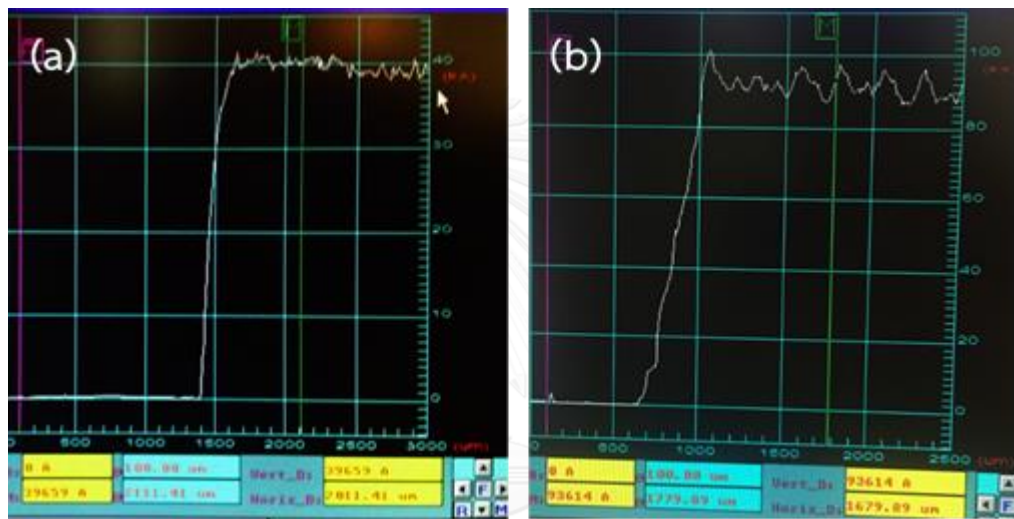


Figure C1. Thickness images of TiO₂ at (a) 1 layer and (b) 3 layers.



APPENDIX D

Data of sheet resistance of modified PMMA sheets

จุฬาลงกรณ์มหาวิทยาลัย
CHULALONGKORN UNIVERSITY

Table D1 Univariate average data for PEDOT on PMMA sheet by spin coating technique

Exp.	Concentrations of EDOT (M)	Volume of EDOT on PMMA sheet (mL)	Spinning rate (rpm)	Spinning time (s)	Layer of EDOT on PMMA sheet	Electrical resistance (R_s) (Ω/cm^2)
EDOT monomer						
1	0.12	0.150	300	30	1	119.4 \pm 1.66
2	0.24	0.150	300	30	1	30.65 \pm 1.39
3	0.72	0.150	300	30	1	48.80 \pm 0.57
Spinning rate						
1	0.24	0.150	300	30	1	30.65 \pm 1.39
2	0.24	0.150	500	30	1	131.6 \pm 5.17
3	0.24	0.150	800	30	1	2,057 \pm 149
4	0.24	0.150	1000	30	1	2,020 \pm 127
Spinning time						
1	0.24	0.150	300	15	1	27.99 \pm 1.54
2	0.24	0.150	300	30	1	30.65 \pm 1.39
3	0.24	0.150	300	45	1	34.10 \pm 0.52
4	0.24	0.150	300	60	1	110.6 \pm 6.92
Layer of EDOT						
1	0.24	0.150	300	30	1	30.65 \pm 1.39
2	0.24	0.150	300	30	2	86.78 \pm 0.08
3	0.24	0.150	300	30	3	91.80 \pm 0.14

Table D2 Effects of 2-methylimidazole concentration on electrical resistance

Exp.	Volume of EDOT on PMMA sheet (mL)	Number layer of EDOT on ZnO/PMMA sheet	Concentration of 2-methylimidazole [M]	Electrical resistance (R_s) (Ω/cm^2)
1	0.150	1	0	30.65 ± 1.39
2	0.150	1	1	33.26 ± 0.02
3	0.150	1	2	28.61 ± 0.96
4	0.150	1	3	19.30 ± 0.13
5	0.015	1	4	10.84 ± 0.09
6	0.150	1	5	12.20 ± 0.18
7	0.150	1	6	61.60 ± 2.14

*Condition: EDOT monomer 0.24 M, spinning time 30 s, spinning rate 300 rpm

Table D3 Effects of ZnO concentration in the PMMA syrup (wt%) on electrical resistance and rms roughness

Exp.	Volume of EDOT on PMMA sheet (mL)	ZnO concentration (wt%)	Layer of EDOT on ZnO/PMMA sheet	Electrical resistance (R_s) (Ω/cm^2)	rms roughness (nm)
1	0.150	0	1	30.65 ± 1.39	23
2	0.150	10	1	31.37 ± 2.52	46
3	0.150	34	1	33.20 ± 2.09	30
4	0.150	58	1	34.16 ± 5.23	32
1	0.150	10	2	38.73 ± 6.41	-
2	0.150	34	2	54.45 ± 6.22	-
3	0.150	58	2	37.99 ± 1.12	-
1	0.150	10	3	36.28 ± 17.2	-
2	0.150	34	3	33.23 ± 11.5	-
3	0.150	58	3	35.24 ± 5.95	-

*Condition: EDOT monomer 0.24 M, spinning time 30 s, spinning rate 300 rpm

The logo of Chulalongkorn University, featuring a central emblem with a sunburst and a tiered structure, surrounded by a circular border.

APPENDIX E

Data of DSSC performance using different counter electrodes

จุฬาลงกรณ์มหาวิทยาลัย
CHULALONGKORN UNIVERSITY

Table E1 I-V characteristics of the cells made with six different counter electrodes

Counter electrode	V_{oc} (mV)	J_{sc} (mA/cm ²)	FF	R_{series} (Ω /cm ²)	P_{max} (mW)	V_{max} (V)	I_{max} (mA)	η (%)
FTO glass ^a	570	0.29	0.07	12,930	0.003	0.12	0.02	0.01
PEDOT/glass ^a	615	0.75	0.26	770.4	0.029	0.32	0.08	0.12
PEDOT/PMMA ^a	695	0.21	0.25	3,219	0.009	0.35	0.03	0.04
2-methylimidazole/ PEDOT/PMMA ^a	680	0.10	0.25	6,329	0.005	0.35	0.01	0.02
PEDOT/10ZnO/PMMA ^a	695	0.55	0.26	1,206	0.025	0.35	0.07	0.10
PEDOT/34ZnO/PMMA ^a	321	0.08	0.26	3,635	0.002	0.16	0.01	0.01
PEDOT/58ZnO/PMMA ^a	585	0.04	0.23	13,110	0.001	0.25	0.006	0.005
2-methylimidazole/ PEDOT/10ZnO/PMMA ^a	670	0.09	0.27	6,548	0.004	0.35	0.01	0.02
PEDOT/10ZnO/PMMA ^b	690	0.47	0.25	1,400	0.020	0.35	0.06	0.08

^aCondition: Dye Z907, liquid electrolyte (HI-30), surlyn 60 μ m, TiO₂ 3 layers (thickness 9 μ m), temperature 120 $^{\circ}$ C, pressure 2 MPa

^bCondition: Dye Z907, gel electrolyte, surlyn 60 μ m, TiO₂ 3 layers (thickness 9 μ m), temperature 120 $^{\circ}$ C, pressure 2 MPa

VITA

Miss Godchaporn Bunmee was born on November 8, 1991 in Rayong, Thailand. She graduated a Bachelor's Degree of Science from Department of Chemistry, Faculty of Science, Mahidol University. She has continued her study in Master's Degree in Petrochemistry and Polymer Science, Program of Petrochemistry and Polymer Science, Faculty of Science, Chulalongkorn University since 2013 and finished her study in 2016.

Presentation

2016 "Enhancement of Electrical Conductivity and UV Stability of Poly(methyl methacrylate) for Dye-Sensitized Solar Cells Application", 8-11 August, Advances in Functional Materials Conference 2016 (AFM 2016) at ICC, Jeju Island, South Korea.

2016 "Electrical Properties Enhancement of Poly(methyl methacrylate) for Dye-Sensitized Solar Cell Application", 26-28 October, The 6th TiChE International Conference 2016 (ITiChE 2016), Bangkok, Thailand. (Gold Poster Presentation Award)